Thermodynamic performance of a novel shell-and-tube heat exchanger incorporating paraffin as thermal storage solution for domestic and commercial applications

Zakir Khan [a,b], Zulfiqar Ahmad Khan [a*]

[a] Bournemouth University, Department of Design & Engineering, NanoCorr, Energy and Modelling (NCEM) Research Group, Fern Barrow, Talbot Campus, Poole, Dorset BH12 5BB, UK.

[b] School of Mechanical & Manufacturing Engineering (SMME), National University of Sciences & Technology (NUST), Sector H-12, Islamabad – 44000, Pakistan.

E-mail: zkhan2@bournemouth.ac.uk

Corresponding Author:

[a*] Bournemouth University, Department of Design & Engineering, NanoCorr, Energy and Modelling (NCEM) Research Group, Fern Barrow, Talbot Campus, Poole, Dorset BH12 5BB, UK.

E-mail: zkhan@bournemouth.ac.uk

Tel.: +44 1202-961645

Abstract

This article is focused to evaluate thermal performance of commercial grade paraffin in a novel shell-and-tube heat exchanger with multi-tube passes and longitudinal fins as latent heat storage (LHS) system. Thermal performance assessments of latent heat storage system are conducted with respects to charging/discharging power, accumulative thermal energy storage/retrieval, thermal efficiencies and effectiveness, heat transfer characterisation and nature of melt front propagation. The average charging and discharging powers are significantly enhanced by 75.53% and 27.04% with an increase in temperature gradient between paraffin and inlet water from 52 °C – 62 °C and 15 °C – 5 °C, respectively. Likewise, the maximum charging and discharging powers are augmented from 2.15 kW – 2.63 kW and 5.18 – 10.37 kW with an increase in flow rate from 1.5 – 3 l/min, respectively. Furthermore, the average effectiveness, Nu-Ra and heat transfer coefficient are significantly improved with an increase in temperature gradient and moderately reduced with upgrading volume flow rate. The range of Rayleigh numbers for charging cycles have indicated turbulent nature of melt front movement and supportive behaviour of longitudinal fins orientations towards natural convection. Empirical correlations for average effectiveness and Nu-Ra are developed from experimental results to facilitate design estimation for employment of proposed LHS systems in domestic and commercial applications. These empirical correlations, to evaluate feasibility and employability of LHS systems in practical applications such as domestic hot water supply and space heating to maintain control room temperature, have been successfully implemented in real operating conditions.

Keywords

Thermal energy storage (TES); Latent heat storage (LHS); Phase change material (PCM); Shell-and-tube heat exchange; Natural convection; effectiveness-NTU

Nomenclature

A_{ext}	External heat transfer surface area (m^2)
C	Constant value
C_p	Specific heat capacity of water $(J/(kg.K))$
$C_{p,HX}$	Specific heat capacity of heat exchanger $(J/(kg.K))$
$C_{p,pcm}$	Specific heat capacity of PCM $(J/(kg.K))$
$D_{T,in}$	Inner diameter of tube (m)
g	Gravitational acceleration (m/s^2)
Gr_L	Grashof number
L	Latent heat capacity of PCM (J/kg)
L_c	Characteristic height (m)
$\dot{m}$	Mass flow rate of water (kg/s)
m_{HX}	Mass of heat exchanger material (kg)
m_{pcm}	Mass of PCM (kg)
Nu	Nusselt number
$\overline{P_c}$	Average charging power (W)
$\overline{P_d}$	Average discharging power (W)
Pr	Prandtl number
Q_c	Thermal energy charged (J)
$Q_{c,max}$	Maximum thermal energy charged (J)
Q_d	Thermal energy discharged (J)
$Q_{d,max}$	Maximum thermal energy discharged (J)
Q_{HX}	Thermal energy stored by heat exchanger (J)
Q_{PCM}	Thermal energy stored by PCM (J)
Ra	Rayleigh number
Re	Reynolds number
Ste	Stefan number
Δt	Time steps to record data (s)
t_c	Complete charging time (s)
t_d	Complete discharging time (s)
T_f	Final temperature of charging cycle (℃)
T_i	Initial temperature of charging cycle (℃)
T_{in}	Inlet temperature of water (℃)
T_m	Phase change temperature of paraffin (℃)
$\overline{T_m}$	Average transient temperature of paraffin (℃)
T_{out}	Outlet temperature of water (℃)
T_s	Surface temperature of the tube (℃)
U	Overall heat transfer coefficient $(W/(m^2.K))$

Greek letters

α	Thermal diffusivity of paraffin (m^2/s)
β	Coefficient of thermal expansion of PCM $(1/K)$
ε	Instantaneous effectiveness
$\overline{\varepsilon_c}$	Average effectiveness of charging cycle
$\overline{\varepsilon_d}$	Average effectiveness of discharging cycle
η_c	Charging efficiency
η_d	Discharging efficiency
v	Kinematic viscosity of paraffin (m^2/s)
μ_w	Dynamic viscosity of water $(Pa.\ s)$

Acronyms

LHS	Latent heat storage
NTU	Number of transfer units
PCM	Phase change material
TES	Thermal energy storage

1. Introduction

The global economic progression and social developments are coupled with higher primary energy supply demands. In the past four decades, the dependency on fossil fuels to meet global energy demands have remained moderately unaffected with an insignificant reduction from 86% to 78.4% [1]. However, the excessive reliance on fossil fuels have resulted in depletion of natural resources and emission of hazardous gases to environment. In order to mitigate global warming and climate change challenges, the development and utilisation of new technologies for renewable energy sources are extremely crucial [2, 3]. Latent heat storage (LHS) systems coupled with solar energy sources or heat recovery systems are appraised as decisive technology to offset mismatch between thermal energy supply and demand. Energy systems yield comparatively better thermal efficiency and sustainability with the integration of LHS systems. Moreover, LHS systems, with their higher thermal storage capacity at almost isothermal condition, wide-ranging availability of phase change materials (PCM), negligible environmental hazards and low vapour pressure encourage practical utilisation in domestic and industrial applications [4-7].

However, the low thermal conductivity of PCMs (≈ 0.2 W/m.K) significantly impedes the thermal efficiency and the large-scale practical applications of LHS systems. Hence, thermal performance enhancement techniques are developed and implemented by researchers to overcome this deficiency. For instance, geometrical orientation of the container, inclusion of extended surfaces with heat exchangers, addition of thermal conductive additives and encapsulation techniques are extensively examined [8-10]. This article will discuss literature concerning shell-and-tube heat exchangers with extended surfaces due to their relatively higher heat transfer potential, minimal design complexity and easier integration to practical applications [11, 12].

Rathod and Banerjee [13] conducted both charging and discharging experimental analyses of stearic acid in a vertical shell-and-tube heat exchanger with three longitudinal fins. It was reported that heat transfer performance at varied operating conditions were improved with inclusion of longitudinal fins. Hence, the charging and discharging rate was significantly enhanced by 24.52% and 43.6%, respectively. Li and Wu [14] informed that with inclusion of six longitudinal fins in a horizontal shell-and-tube heat exchanger, the average heat flux was significantly enhanced and consequently, the charging and discharging rate was enhanced by 14% as compared to the no-fins configuration. Ye [15] conducted numerical simulation of paraffin in horizontal double tube heat exchanger with varying longitudinal fins from 0 – 10. It was reported that as compared to no-fins orientation, the melting time was significantly reduced by 40% – 86% with an increase in longitudinal fins from 2 – 10, respectively. In another study, Ye [16] numerically examined the optimal aspect ratio for melting process of paraffin in vertically heated rectangular container. It was concluded that melting process can be augmented with an increase in aspect ratio from 0.1 – 1 and the optimal melting performance can be achieved for aspect ratio ≥ 1. Similarly, Rabienataj Darzi et al. [17] numerically investigated the thermal behaviour of n-eicosane in a horizontal shell-and-tube heat exchanger with varying number of longitudinal fins. It was noticed that as compared to the no-fins configuration, an increase in longitudinal fins from 4 – 20 significantly enhanced the charging rate by 39% – 82% and discharging rate by 28% – 85%, respectively. Thermal performance enhancements with inclusion of longitudinal fins were more effective in discharging cycles due to the fact that higher numbers of extended surfaces obstruct effective natural convection during charging cycles. Moreover, Lohrasbi et al. [18] conducted numerical evaluation of thermal performance of PCM in a vertical shell-and-tube heat exchanger with no-fin, longitudinal fin and circular fin orientations. Longitudinal and circular fins augmented the thermal penetration depth and consequently, the phase transition rate was enhanced by 3.26 and 3.55 times, respectively. Caron-Soupart et al. [19] performed experimental analyses on paraffin in three configurations of a shell-and-tube heat exchanger with no-fins, longitudinal fins and circular fins. It was reported that longitudinal and circular fins had improved thermal power by a factor of 10. Moreover, the role of natural convection on temperature distribution during charging process was significant. Kabbara et al. [20] experimentally examined the charging and discharging behaviour of dodecanoic acid in a vertical shell-and-tube heat exchanger with rectangular fins and four tube passes. It was recorded that the average power was merely increased from 0.24 – 0.32 kW with an increase in volume flow rate from 0.7 – 2.5 l/min. It can be noticed from the literature review that a single tube pass of a shell-and-tube heat exchanger with longitudinal fins are extensively investigated both numerically and experimentally. However, the literature lacks thermal evaluation of shell-and-tube heat exchangers with multi-tube passes and longitudinal fins with relatively higher thermal storage capacity to support integration into practical applications. Therefore, a novel geometrical configuration of a shell-and-tube heat exchanger with multi-tube passes and longitudinal fins was previously designed and optimised in [21], developed and experimentally examined for charging and discharging cycles in [22, 23]. The experimental evaluations were focused on vertical and radial temperature distributions, and melting and solidification rates of paraffin in the proposed design solution.

In past decade, the inclusion of thermal conductive additives are extensively investigated for their potential to improve thermal performance of LHS systems [24]. Yang et al. [25] conducted numerical investigations on metal foam enhanced paraffin in vertical shell-and-tube heat exchanger. It was reported that with inclusion of metal foam (copper) in paraffin with optimal porosity of 0.94, the melting rate was significantly augmented by 88.54% as compared to no metal foam enhanced paraffin. Yang et al. [26, 27] furthered the numerical analyses by probing the impacts of natural convection and angles of inclination of container on charging rates of metal foam based paraffin composite. It was reported that natural convection based numerical simulations had presented significantly higher phase transition rates (45.5%) as compared to conduction dominant simulations. Moreover, due to excellent temperature distribution in metal foam enhanced paraffin, the angles of inclination had demonstrated minimal enhancement of 4.35% between cases with angles $0°$ and $90°$. In other words, the natural convection has minimal influence on phase transition process in metal foam enhanced LHS systems and the uniform temperature distributions were owing to conduction dominance. Mahdi and Nsofor [28] reported similar observations in their numerical examination of metal foam enhanced PCM in horizontal shell-and-tube heat exchanger. Meng and Zhan [29] conducted experimental charging and discharging cycles on copper foam enhanced paraffin in vertical shell-and-tube heat exchanger. It was reported that the charging power was improved from 0.13 kW to 0.22 kW with an increase in inlet temperature from 75 ^{o}C to 85 ^{o}C. Likewise, the discharging power was enhanced from 0.17 kW to 0.27 kW with reducing the inlet temperature from 20 ^{o}C to 10 ^{o}C, respectively. Furthermore, the inclusion of metal oxides (Al_2O_3), metal nitrides (AlN) and carbon allotropes (GNP) based nano-additives to paraffin in horizontal shell-and-tube heat exchanger was experimentally and numerically investigated in [30]. It was reported that as compared to pure paraffin, the charging rates for Al_2O_3, AlN and GNP based nano-PCMs were significantly enhanced by 28.01%, 36.47% and 44.57%, and the discharging rates by 14.63%, 34.95% and 41.46%, respectively. However, it was reported in [31-34] that as compared to thermal conductive additives enhanced LHS systems, the phase transition rates and thermal storage capacities of LHS systems with optimised extended surfaces were relatively higher.

Effectiveness-NTU is considered as a decisive technique for characterising and evaluating heat transfer performance for specific designs of LHS systems [35]. This technique is implemented by researchers to assess and optimise thermal performance of proposed design solutions of LHS systems. Tay et al. [36] conducted experimental and numerical analyses on enhancement in average effectiveness and phase change rate of PCM in LHS system with no-fins, pins and circular fins orientations. It was reported that amongst 16 tubes orientations with similar volumes, the tube with circular fins presented higher average effectiveness and rapid phase change rate as compared to no-fins and pins orientations. It was due to relatively higher effective surface area of circular fins which enabled the enhancement in average effectiveness and phase change rates by 20 – 40 % and 25 % as compared to no-fins orientation, respectively. Moreover, the empirical correlations for effectiveness as a function of effective surface area and operating mass flow rate of HTF are developed in [37-40]. Despite being significantly influential parameters, the literature lacks consideration of operating inlet temperature and phase change temperature of PCM while developing empirical correlations for average effectiveness. Furthermore, the previous literature do not consider in-depth evaluation of design configurations impacts on natural convection and nature of melt front propagation.

This article is the continuation of experimental thermal performance evaluation of the novel LHS system in terms of comprehensive transient and average charging/discharging power, accumulative thermal energy storage/retrieval, charging/discharging thermal efficiencies, average effectiveness assessment and natural convection characterisation at varied operating conditions. Thermal performance evaluations of proposed novel LHS system are based on experimental data acquired from twenty-eight charging and discharging cycles, which is symbolic and unprecedented contribution to literature. The above-mentioned thermal performance evaluations have not been considered or published in our earlier articles [21-23]. Moreover, this article is focused on developing empirical correlations for charging and discharging effectiveness, which will empower to evaluate the design characterisation and employability of this novel LHS system in practical applications. The empirical correlations are derived which considers parameters for inlet temperature and flow rate of heat transfer fluid (water), phase change temperature of paraffin (or other PCM) and effective external surface area of the heat exchanger. The developed empirical correlations are unique in terms of empowering implementation for a range of phase change materials and varied operating conditions of heat transfer fluid, which are not reported in previous literature. Moreover, the average effectiveness of the proposed novel LHS system is compared with other published designs. Similarly, the impact of natural convection on heat transfer and melt front propagation of paraffin in novel design configuration are characterised by evaluating Nusselt number (Nu) and Rayleigh number (Ra). An empirical correlation is developed for Nu-Ra and compared with established results in literature. The practicality and viability of proposed LHS system integration to domestic and commercial applications are evaluated by conducting two case studies.

2. Experimental setup and procedure

2.1. Experimental setup

The experimental test rig is demonstrated in a schematic diagram, as shown in **Fig. 1**. The test rig consists of a flat plate solar collector setup with solar simulators, latent heat storage (LHS) system, connection to the municipal water supply, centrifugal pump, flow control valves and data acquisition system with computer.

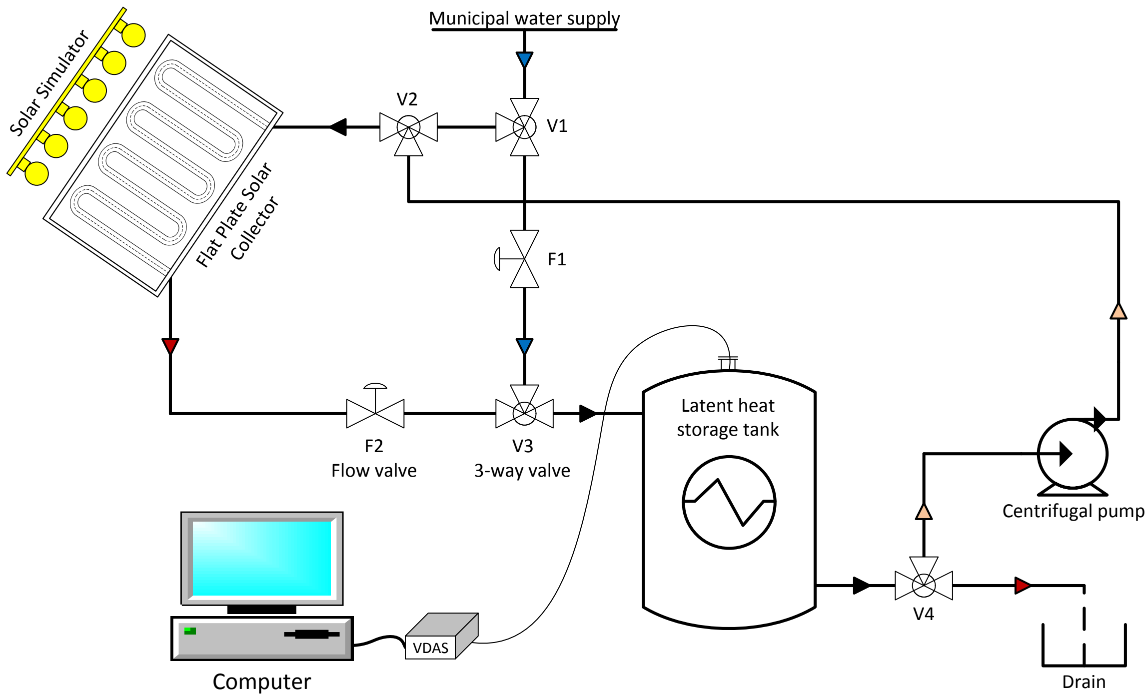

Fig. 1 Schematic representation of experimental test rig for charging/discharging cycles of LHS system coupled with flat plate solar collector.

To conduct charging cycles, the water supply is directed to pass through serpentine copper tubing in the solar collector, where steady radiant thermal energy from solar simulators is absorbed by the water. The technical specifications and operation details of the solar simulators based solar collector system is discussed comprehensively in [22, 41], as presented in Table 1. The high temperature water at the solar collector outlet is directed to pass through the LHS tank, where heat transfer occurs between high temperature water in the tubes and paraffin in the shell container. Thermal energy is transmitted to the paraffin in the shell container and therefore, the low temperature water at the LHS outlet is pumped back to the solar collector to repeat the charging process. Technical design specifications of shell-and-tube heat exchanger with multi-tube passes and longitudinal fins are previously discussed and detailed in [21, 22], as shown in Table 2. Likewise, the physical model of the LHS unit is illustrated in Fig. 2 and the thermo-physical properties of commercial grade paraffin (RT44HC) are presented in Table 3. Technical limitations of lab-scale solar collector system are considered while selecting the appropriate range of phase transition temperature of paraffin. Hence, in case of larger solar collector, the paraffin with higher phase transition temperature can be utilised in this novel designed LHS system.

A Grundfos centrifugal pump (UPS 15-60) is employed to circulate water in a closed loop between the solar collector and the LHS unit. Moreover, four 3-way valves are installed to conduct charging/discharging cycles by adjusting flow direction and operating volume flow rate. FT2 turbine flow meters are utilised to record volume flow rates of the water. Furthermore, to record thermal response of the paraffin in the shell container to inlet temperature of the water, fifteen K-type thermocouples are installed at five zones (A, B, C, D and E) and at three vertical positions (top, central and bottom) at each zone, as illustrated in Fig. 2. The vertical positions of thermocouples are at a vertical distance of 115 mm to each other. Also, two K-type thermocouples are coupled to the copper tube at the inlet and outlet of the LHS unit to register temperature response of the water. The accuracy of the turbine flow meters and thermocouples are 1.5% and ±1.5 ^{o}C, respectively. An Agilent data acquisition (34972A) unit is connected to the sensors to aquire temperature and volume flow rates data. Agilent software is operated to log temperature and volume flow rates data at time steps of 10 s.

Table 1
Technical specifications of FPSC coupled with solar simulator [22, 41]

Components	Parameters	Value
Gross Dimensions	Length (m)	2.4
	Width (m)	2.9
	Thickness (m)	0.254
Glazing	Material	Transparent glass
	Thickness (m)	0.002
	Emissivity	0.92
	Transmittance	0.9
Absorber	Material	Stainless steel S280
	Coating	Dark black surface
	Thickness (m)	0.001
	Thermal Conductivity (W/(m.K))	50
	Absorptivity	0.9
	Emissivity	0.9
Circulation System	Material	Copper
	Running Length (m)	57.5
	Length of each Segment (m)	2.5
	Number of Segments	23
	Outer diameter (m)	0.01
	Inner diameter (m)	0.008
	Thermal Conductivity (W/(m.K))	300
Back Insulation	Material	Celotex
	Thickness (m)	0.1
	Thermal Conductivity (W/(m.K))	0.022
Solar Simulator	Type of lamps	Quartz-halogen
	Number of lamps	12
	Radiant heat output per lamp (kW)	1
	Distance from collector (m)	2

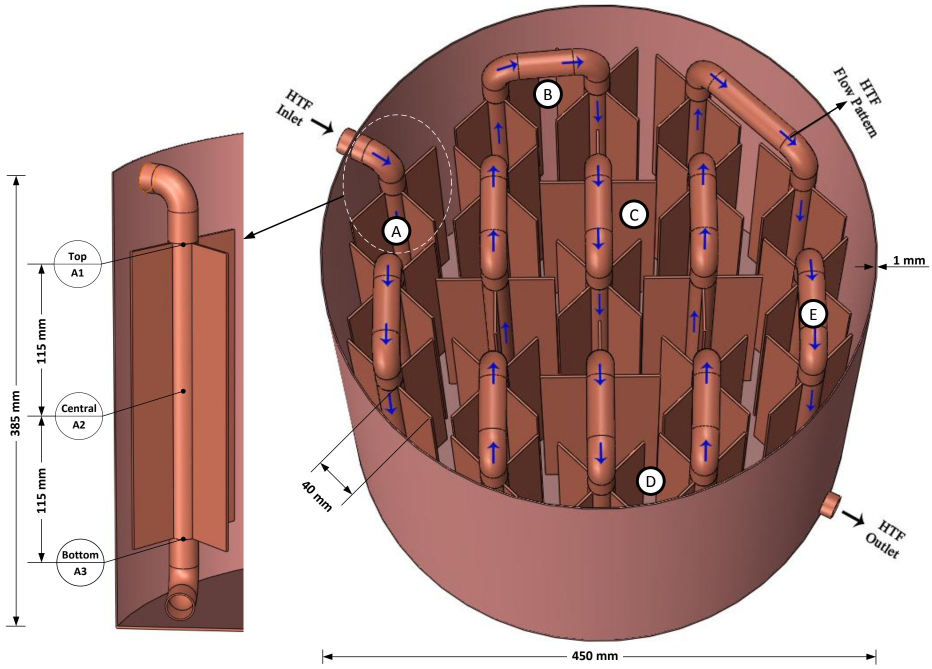

Fig. 2 Physical model illustration of the shell-and-tube heat exchanger with multi-tubes and longitudinal fins based LHS unit and vertical and radial positioning of thermocouples in shell container [22].

Table 2
Technical specifications of shell-and-tube heat exchanger based LHS unit used in test rig [21, 22]

Components	Parameters	Value
Shell	Material	Copper
	Height (m)	0.385
	Outer diameter (m)	0.450
	Inner diameter (m)	0.448
	Volume of shell (m^3)	0.0607
Tube	Material	Copper
	Height of each tube pass (m)	0.320
	Number of passes	21
	Outer diameter (m)	0.022
	Inner diameter (m)	0.020
	Running length (m)	8.2
	Volume of tube (m^3)	0.00312
Fins	Material	Copper
	Height (m)	0.230
	Length (m)	0.04
	Thickness (m)	0.0015
	Number of fins	76
	Volume of fins (m^3)	0.00105
Insulation	Material	CFC-free envirofoam
	Thickness (m)	0.05
PCM and HTF	HTF Material	Water
	PCM Material	Paraffin (RT44HC)
	Mass of PCM (kg)	40
	Packing factor of PCM	0.824 (Solid) 0.942 (Liquid)

Table 3
Thermo-physical characteristics of paraffin as PCM, copper as construction material for shell-and-tube heat exchanger and water as HTF [42, 43]

Parameters	Paraffin (RT44HC)	Copper	Water
Phase change temperature (^{o}C)	41-44	1083	0-4
Latent heat capacity (kJ/kg)	255	0.205	333.5
Density (kg/m^3)	800 at 20 ^{o}C 700 at 80 ^{o}C	8960 at 25 ^{o}C 8935 at 70 ^{o}C	999.93 at 5 ^{o}C 977.75 at 70 ^{o}C
Specific heat capacity (kJ/(kg.K))	2.0	0.385	4.204 at 5 ^{o}C 4.189 at 70 ^{o}C
Thermal conductivity (W/(m.K))	0.2	398	0.571 at 5 ^{o}C 0.663 at 70 ^{o}C
Coefficient of thermal expansion (1/K)	3 x 10^{-4}	0.167 x 10^{-4}	0.114 x 10^{-4} at 5 ^{o}C 5.71 x 10^{-4} at 70 ^{o}C

2.2. Experimental procedure

Prior to conducting charging cycles, the low temperature water is circulated through the serpentine tubing in the solar collector and multi-tube passes in the LHS unit to ensure good baseline initial temperature and to release trapped air in the loop. Initial temperature of the paraffin in the shell container of the LHS unit is maintained at 10 ^{o}C. Three-way valves are adjusted to regulate flow direction between the solar collector and the LHS unit for operating closed loop charging cycles.

Solar simulators are used to direct radiant heat at the solar collector. Water absorbs thermal energy while passing through the serpentine tubing in the solar collector and therefore, the temperature of water is increased from initial ambient to the selected range. The high temperature water at the outlet of the solar collector is directed to pass through multi-tube passes in the LHS unit where thermal energy is transferred to low temperature paraffin. Paraffin absorbs thermal energy and phase transition from solid to liquid starts. The low temperature water at the outlet of the LHS unit is pumped back to the solar collector to continue closed loop charging cycle. Charging cycle is continued until all fifteen thermocouples in the shell container of the LHS unit register temperature higher than phase change temperature of the paraffin.

Likewise, in the case of discharging cycles, it is ensured that the entire mass of paraffin is in liquid state and the thermocouples installed at top position at all zones in the shell container register paraffin temperature equal to 52 ^{o}C. Three-way valves are adjusted again to regular flow direction for open loop discharging cycle between the water supply and the LHS unit. The solar collector and centrifugal circulation pump are bypassed in discharging cycles.

In discharging cycles, the low temperature water is directed to pass through the LHS unit. Heat transfer occurs between low temperature water in multi-tube passes and high temperature paraffin in the shell container. Paraffin enthalpy drops and hence phase transition initiates from liquid to solid state. High temperature water at the outlet of the LHS unit can be consumed and is desirable for domestic or industrial applications. The discharging cycle is continued until all fifteen thermocouples in the shell container register temperature lower than the phase change temperature of paraffin and the temperature gradient between the inlet and outlet of the water is less than 5 ^{o}C. The range of experimental tests conducted on charging and discharging cycles at varied operating conditions of temperature and volume flow rates is presented in Table 4.

Table 4
Range of charging/discharging cycles conducted at varied operating conditions

	Set of Experiments	Inlet Temperature (°C)	Stefan No	Reynolds No			
				1.5 l/min	2.0 l/min	2.5 l/min	3.0 l/min
Charging cycle	1-4	52	0.078	2950	4000	4950	5900
	5-8	57	0.118	3200	4300	5350	6400
	9-12	62	0.157	3450	4600	5750	6900
	13-16	67	0.196	3700	4900	6150	7400
Discharging cycle	17-20	5	0.290	1050	1395	1745	2100
	21-24	10	0.251	1220	1625	2030	2435
	25-28	15	0.212	1400	1865	2330	2800

3. Thermal performance evaluation

The flow regime of water in multi-tube passes in the LHS unit at varied operating conditions is determined using Reynolds number (Re) as follow [44]:

$$Re = \frac{4\dot{m}}{\pi D_{T,in} \mu_w} \quad (1)$$

where $\dot{m}, \mu_w$ and $D_{T,in}$ represent mass flow rate of water (kg/s), dynamic viscosity of water at inlet temperature (Pa. s) and inner diameter of tube (m). In case of phase transition, the ratio between sensible and latent heat is evaluated through Stefan number (Ste), as follow [45]:

$$Ste = \frac{C_{p,pcm}\, \Delta T_{Ste}}{L} \quad (2)$$

where $C_{p,pcm}$, L and ΔT_{Ste} represent the specific heat capacity of paraffin (J/(kg.K)), latent heat capacity of paraffin (J/kg) and temperature gradient between phase transition temperature of paraffin and inlet temperature of water (°C), respectively. Table 4 presents the nature of flow regime and Stefan number for each experimental test.

3.1. Thermal energy and mean power evaluation

Thermal energy charge Q_c (J) and discharge Q_d (J) by the paraffin in the shell container is equated from the energy balance equation for inlet and outlet enthalpy change of water, as follows:

$$Q_c = \sum_{t=0}^{t_c} \dot{m} \left(\frac{C_{p,in} + C_{p,out}}{2} \right) (T_{in} - T_{out}) \Delta t \quad (3)$$

$$Q_d = \sum_{t=0}^{t_d} \dot{m} \left(\frac{C_{p,in} + C_{p,out}}{2} \right) (T_{out} - T_{in}) \Delta t \quad (4)$$

where $\dot{m}, C_p, T_{in}, T_{out}$ and Δt represent the mass flow rate of water (kg/s), specific heat capacity of water at inlet and outlet (J/(kg.K)), temperature of water at inlet and outlet (°C) and time step to register data (s). Likewise, the instantaneous charging/discharging power can be equated by dividing Eq. 3 and Eq. 4 with Δt. Moreover, the average charging power $\overline{P_c}$ (W) and discharging power $\overline{P_d}$ (W) can be calculated as follows:

$$\overline{P_c} = \frac{Q_c}{t_c} \tag{5}$$

$$\overline{P_d} = \frac{Q_d}{t_d} \tag{6}$$

where t_c and t_d represent complete charging and discharging time of paraffin, respectively.

3.2. Charging and discharging cycles efficiency

The charging and discharging cycle efficiencies indicators are introduced to evaluate thermal behaviour of the LHS unit at varied operating conditions, as follows:

$$\eta_c = \frac{Q_c}{Q_{c,max}} \tag{7}$$

$$\eta_d = \frac{Q_d}{Q_{d,max}} \tag{8}$$

where η_c and η_d symbolise charging and discharging efficiency, respectively. $Q_{c,max}$ and $Q_{d,max}$ represents maximum theoretical thermal energy charged/discharged by the LHS unit. As discussed earlier, the LHS unit is comprised of a shell-and-tube heat exchanger with longitudinal fins and paraffin as thermal storage material, therefore the overall thermal energy storage is equated as the collective thermal energy stored by heat exchanger and paraffin, as follows:

$$Q_{c,max} = Q_{HX} + Q_{PCM} \tag{9}$$

$$Q_{HX} = m_{HX} C_{p,HX} (T_i - T_f) \tag{10}$$

$$Q_{PCM} = \int_{T_i}^{T_m} m_{pcm} C_{p,pcm} dT + m_{pcm} L + \int_{T_m}^{T_f} m_{pcm} C_{p,pcm} dT \tag{11}$$

where m_{HX}, $C_{p,HX}$, T_i and T_f shows mass of copper used in heat exchanger (kg), specific heat capacity of copper (J/(kg.K)) and initial and final temperature of charging/discharging cycle (^{o}C), respectively. Likewise, m_{pcm} and T_m represents mass of paraffin in the shell container (kg) and phase change temperature of paraffin (^{o}C).

3.3. Effectiveness-NTU method

The design and thermal performance analysis are conducted by implementing effectiveness-NTU method. Effectiveness equates to the ratio between actual heat charged or heat discharged over maximum possible heat charged or heat discharged during phase change duration, as given [46]:

$$\varepsilon = \frac{T_{in} - T_{out}}{T_{in} - \overline{T_m}} \tag{12}$$

Eq. (12) evaluates instantaneous effectiveness over the period of phase change. In this article, the average transient temperature plot for paraffin is produced from all fifteen local temperatures and accordingly $\overline{T_m}$ represents the average transient temperature of paraffin during phase change period. Due to transient nature of effectiveness, the output values are limited between 0 and 1. Similarly, the average charging/discharging effectiveness during the phase change period can be calculated as follows [38]:

$$\overline{\varepsilon_c} = \frac{1}{t_c}\sum_{t=0}^{t_c} \varepsilon_c \quad (13)$$

$$\overline{\varepsilon_d} = \frac{1}{t_d}\sum_{t=0}^{t_d} \varepsilon_d \quad (14)$$

Average effectiveness is correlated to average number of transfer units (NTU) of the LHS unit, which evaluates the average thermal resistance to heat transfer between water and phase change front of paraffin, as given [47]:

$$\bar{\varepsilon} = 1 - \exp(-NTU) \quad (15)$$

$$\bar{\varepsilon} = 1 - \exp\left(\frac{-UA_{ext}}{\dot{m}C_p}\right) \quad (16)$$

where U and A_{ext} indicate overall heat transfer coefficient (W/(m^2.K)) and effective external heat transfer surface area (m^2), respectively. Eq. (16) indicates average effectiveness as a function of mass flux. Further details regarding average effectiveness and mass flux relation could be found in [38, 39, 48, 49]. Similarly, a generalised correlation of Eq. (16) is established as follows:

$$\bar{\varepsilon} = 1 - \exp\left(-C.\left(\frac{A_{ext}}{\dot{m}}\right)\right) \quad (17)$$

where C is a constant that specifies heat charging/discharging performance of the LHS unit.

3.4. Evaluation of natural convection

To evaluate the impact of varying operating conditions on dominating mode of heat transfer between water and paraffin, the non-dimensional Rayleigh number (Ra) and Nusselt number (Nu) are implemented. Rayleigh number accounts for buoyancy driven flow, natural convection and nature of phase front moment (laminar or turbulent), as given [44]:

$$Ra = Gr_L Pr = \frac{g\beta(T_s - \overline{T_m})L_c{}^3}{v\alpha} \quad (18)$$

where g, β, T_s, L_c, v and α symbolise gravitational acceleration (m/s^2), coefficient of thermal expansion of paraffin (1/K), surface temperature of the tube ($T_s = (T_{in} + T_{out})/2$), characteristic height of tube with longitudinal fins (m), kinematic viscosity of paraffin (m^2/s) and thermal diffusivity of paraffin (m^2/s), respectively. Tubes surfaces with longitudinal fins are treated as vertical plates for calculating Ra. Therefore, the characteristic height is considered equivalent to the height of each tube pass i.e. 0.32 m. Transient kinematic viscosity of paraffin is determined by implementing the following relation [50]:

$$v = \frac{\mu}{\rho} = \frac{1}{\rho}\left(0.001exp\left(-4.25 + \frac{1790}{\overline{T_m}}\right)\right) \quad (19)$$

The nature of phase front moment of paraffin in shell container is laminar for Rayleigh number in the range of $(10^4 \leq Ra \leq 10^9)$ and turbulent for $(Ra \geq 10^9)$ [44]. Moreover, Churchill and Chu [51] derived a correlation for local Nusselt number and Rayleigh number, as follows:

$$Nu = \left\{0.825 + \frac{0.387Ra^{1/6}}{(1+(0.492/Pr)^{9/16})^{8/27}}\right\}^2 \tag{20}$$

Similarly, the average values for Rayleigh number and Nusselt number of paraffin in a shell container over the period of charging cycles are calculated by follow relations:

$$\overline{Ra} = \frac{1}{t_c}\sum_{t=0}^{t_c} Ra \tag{21}$$

$$\overline{Nu} = \frac{1}{t_c}\sum_{t=0}^{t_c} Nu \tag{22}$$

An empirical correlation between $\overline{Ra}$ and $\overline{Nu}$ is generated based on experimental results, in the following form:

$$\overline{Nu} = C\overline{Ra}^n \tag{23}$$

4. Results and Discussion

4.1. Repeatability and uncertainty analysis

To ensure repeatability of experimental results, three charging cycles are conducted at constant operating conditions of water. Inlet temperature and volume flow rate are set constant to 62 ^oC and 1.5 l/min, respectively. Transient temperature profiles of paraffin in the shell container acquired from thermocouples are averaged and plotted against charging time, as shown in Fig. 3 (A). Likewise, the transient variations in temperature plots of inlet and outlet temperatures of water are illustrated in Fig. 3 (B). It can be noticed that the average temperature profiles of paraffin and inlet/outlet temperature plots of water for all three experiments are almost identical. The experimental results validate good reliability and repeatability of thermal performance of LHS system with average standard deviation values of 0.49, 0.38 and 0.52 for average temperatures of paraffin, inlet and outlet temperatures of water, respectively.

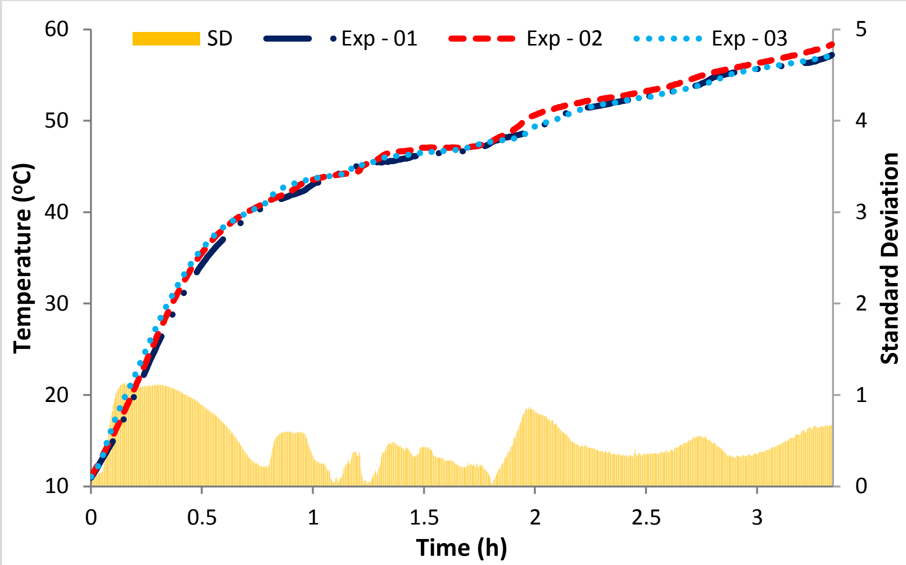

(A)

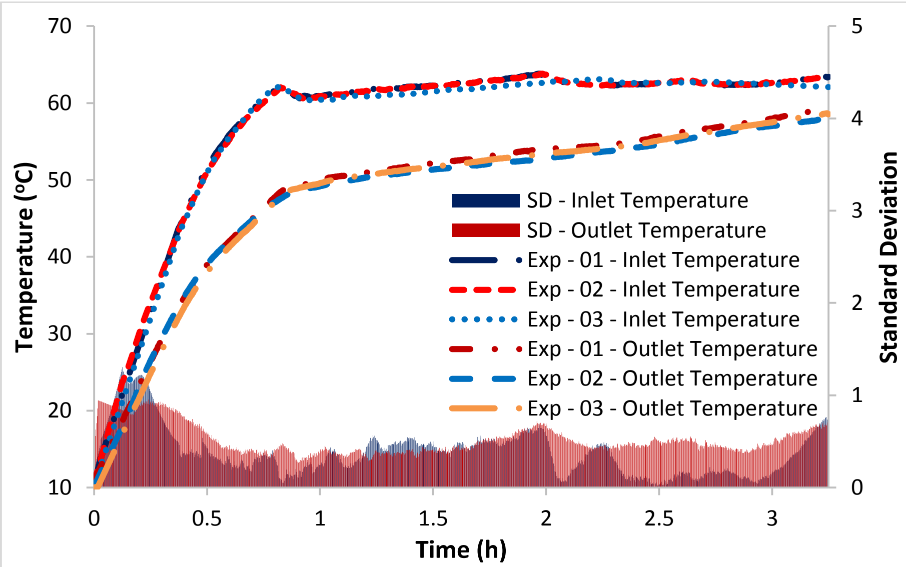

(B)

Fig. 3 Repeatability demonstration of average temperature of paraffin (A) and inlet/outlet temperatures of water (B) while charging at constant inlet temperature of 62 ºC and volume flow rate of 1.5 l/min.

The experimental errors associated with the uncertainties of measuring thermocouples and flow meter readings are determined by implementing Kline-McClintock's model [52, 53]. Hence, the propagation of uncertainties in measured and calculated thermal performance parameters of LHS system are evaluated by identifying the uncertainties of all independent variables, as follow [52, 54]:

$$R = f(x_1, x_2, x_3, \dots, x_n) \tag{24}$$

$$\delta R = \sqrt{\left(\frac{\partial R}{\partial x_1}\delta x_1\right)^2 + \left(\frac{\partial R}{\partial x_2}\delta x_2\right)^2 + \left(\frac{\partial R}{\partial x_3}\delta x_3\right)^2 + \dots + \left(\frac{\partial R}{\partial x_n}\delta x_n\right)^2} \tag{25}$$

where R represents the thermal performance parameter which is influenced by several independent variable i.e. $x_1, x_2, x_3, \ldots, x_n$. Similarly, δR and $\delta x_1, \delta x_2, \delta x_3, \ldots, \delta x_n$ symbolise the uncertainty of thermal performance parameter and uncertainties of all independent variables, respectively. Thus, the maximum percentage uncertainties propagated in the experimental results of thermal energy charged and discharged are 6.1% and 4.8%, in effectiveness of charging and discharging cycles are 3.0% and 3.1%, in Rayleigh number and Nusselt number are 4.3% and 5.6%, respectively.

4.2. Charging power and energy stored

To conduct charging cycles, the high temperature water from the solar collector is directed to pass through multi-tube passes where thermal energy is transferred to low temperature solid paraffin in the shell container. Due to thermal energy storage, solid paraffin engages in phase transition to a liquid state. Transient local temperature responses of the paraffin are recorded by fifteen thermocouples installed in the shell container and are extensively discussed in [22]. Table 4 represents the set of sixteen charging cycles conducted at varied operating temperatures and volume flow rates.

Transient charging power of paraffin is evaluated by registering instantaneous rate of change in enthalpy of water at inlet and outlet, as presented in Fig. 4. Transient charging power can be categorised into three stages: rapid increase at initial stages until it reaches the maximum value, brief sharp declination and gradual declination or almost uniform charging power up until the end of charging cycle. It can be construed that conduction heat transfer is the dominant mode of heat transfer at initial stages of the charging cycle. Moreover, due to the relatively higher temperature gradient between the inlet water and the paraffin at initial stages, the maximum value of charging power is reached. In the second stage, the brief sharp declination demonstrates the onset of phase transition of the paraffin to a liquid state. In the third stage, natural convection starts dominating the charging process. Furthermore, due to continued increase in paraffin temperature, the thermal gradient between water and paraffin reduces which results in gradual decline in charging power.

The impact of varying operating conditions on charging power is pronounced, as shown in Fig. 4. It can be noticed from Fig. 4 (A) that at constant inlet temperature of 52 ^{o}C and increasing volume flow rate from 1.5 l/min to 3 l/min, the maximum charging power is augmented from 1.48 kW to 2.39 kW, respectively. Likewise, in the case of 57, 62 and 67 ^{o}C, the maximum charging power is improved from 1.38 – 1.98 kW, 1.54 – 1.97 kW and 2.15 – 2.63 kW, respectively (see Fig. 4 (B), (C) and (D)). Moreover, the average charging power at varied operating conditions is illustrated in Fig. 4 (E). It is evident that with an increase in operating inlet temperature of water, the average charging power is significantly improved. For instance, with an increase in inlet temperature from 52 ^{o}C to 57, 62 and 67 ^{o}C and constant volume flow rate of 3 l/min, the average power is enhanced by 22.39%, 75.53% and 76.41%, respectively. Furthermore, it is observed that the average charging power does not exhibit significant enhancement with an increase in inlet temperature of the water from 62 ^{o}C to 67 ^{o}C.

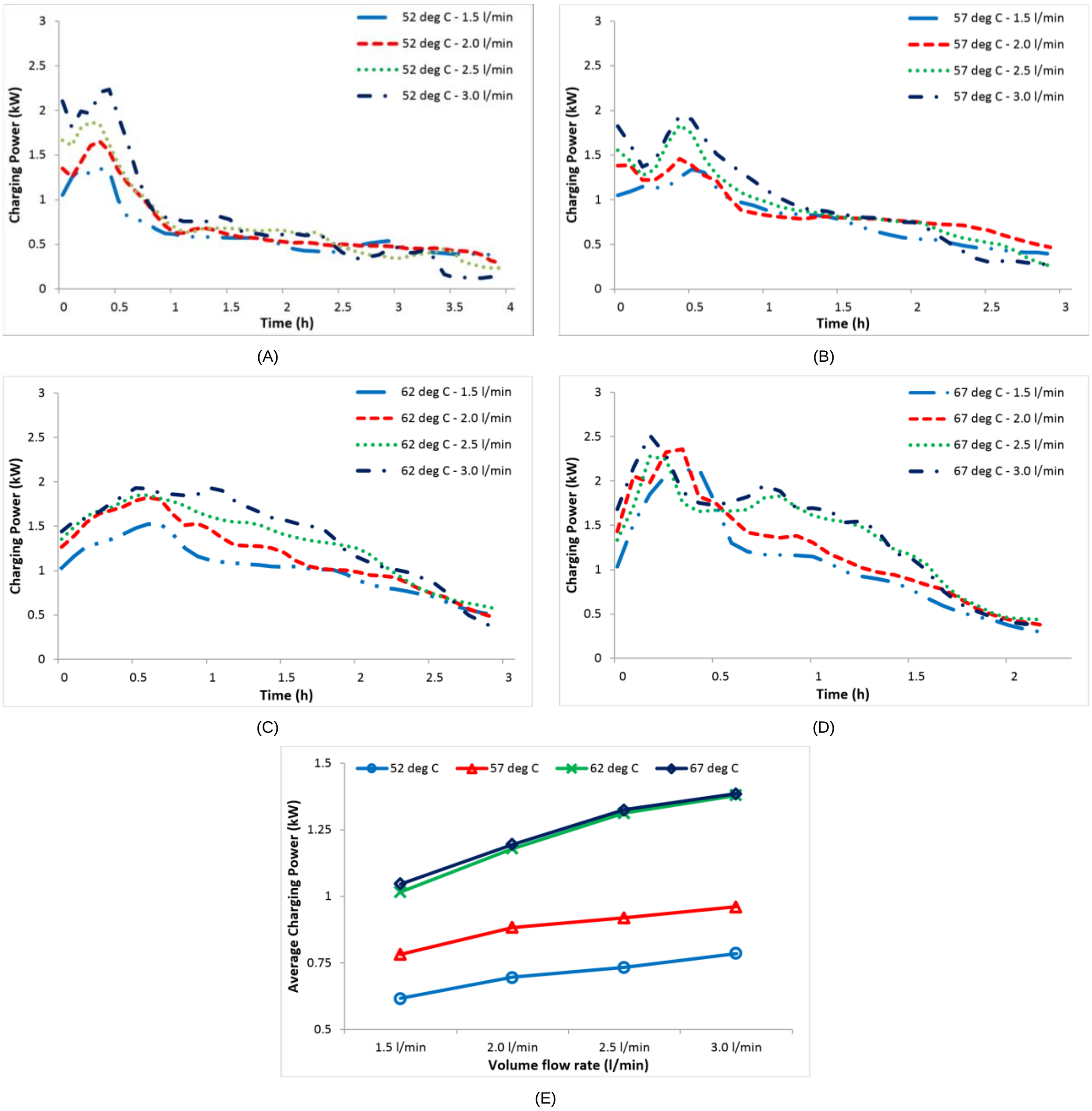

Fig. 4 Transient and average charging power of LHS unit while conducting experimental charging cycles at varied operating conditions.

Similarly, the accumulative thermal energy storage by paraffin in the LHS unit is assessed for all sixteen charging cycles at varied operating conditions, as presented in Fig. 5. It can be observed that the higher charging power at initial stages of charging cycle enables maximum accumulation of thermal energy. It is depicted by a linear increment in accumulative energy storage versus time. Further on, the charging power is continuously and gradually declining towards later stages of charging cycle which results in slower accumulation of thermal energy storage, as illustrated by curved increments.

Fig. 5 demonstrates the influence of varying operating conditions on accumulative thermal energy storage. It can be noticed that while charging at constant inlet temperature and varying volume flow rate from 1.5 l/min to 3 l/min, the turbulent nature of water in the multi-tube passes increases which improves heat transfer to the paraffin in the shell container and consequently, the rate of accumulative thermal energy storage is increased. Also, an increase in volume flow rate of the water ensures a rise in average multi-tube wall temperature. In the case of charging for 4 h at constant inlet temperature of 52 ^{o}C, the accumulative energy storage is improved by 11.78%, 18.55% and 23.68% with an increase in volume flow rate from 1.5 l/min to 2, 2.5 and 3 l/min, respectively (see Fig. 5 (A)). Similarly, while charging for 3 h at constant inlet temperature of 62 ^{o}C, the accumulative energy storage is enhanced by 15.28%, 29.64% and 35.61%, respectively (see Fig. 5 (C)). However, while charging for 2.5 h at constant inlet temperature of 67 ^{o}C, an augmentation of a mere 3.03%, 6.11% and 10.61% is noticed, respectively (see Fig. 5 (D)). It is due to the fact that at higher inlet temperature, the average multi-tube wall temperature is insignificantly influenced by increasing the volume flow rate of the water. Furthermore, the effect of increasing inlet temperature and constant volume flow rate on thermal energy storage is illustrated in Fig. 5 (E). It can be observed that while charging for 3 h, the amount of thermal energy charged is significantly improved from 7.42 MJ to 8.48, 11.07 and 12.76 MJ as the inlet temperature is increased from 52 ^{o}C to 57, 62 and 67 ^{o}C, respectively. In other words, an enhancement of 14.24%, 49.25% and 72.17% is achieved with an increase in inlet temperature, respectively.

Therefore, an increase in inlet temperature of water has more pronounced impact on charging power and accumulative thermal energy storage of paraffin as compared to increasing volume flow rate. Hence, an increase in Stefan number has more significant impact on charging cycles as compared to increasing Reynolds number.

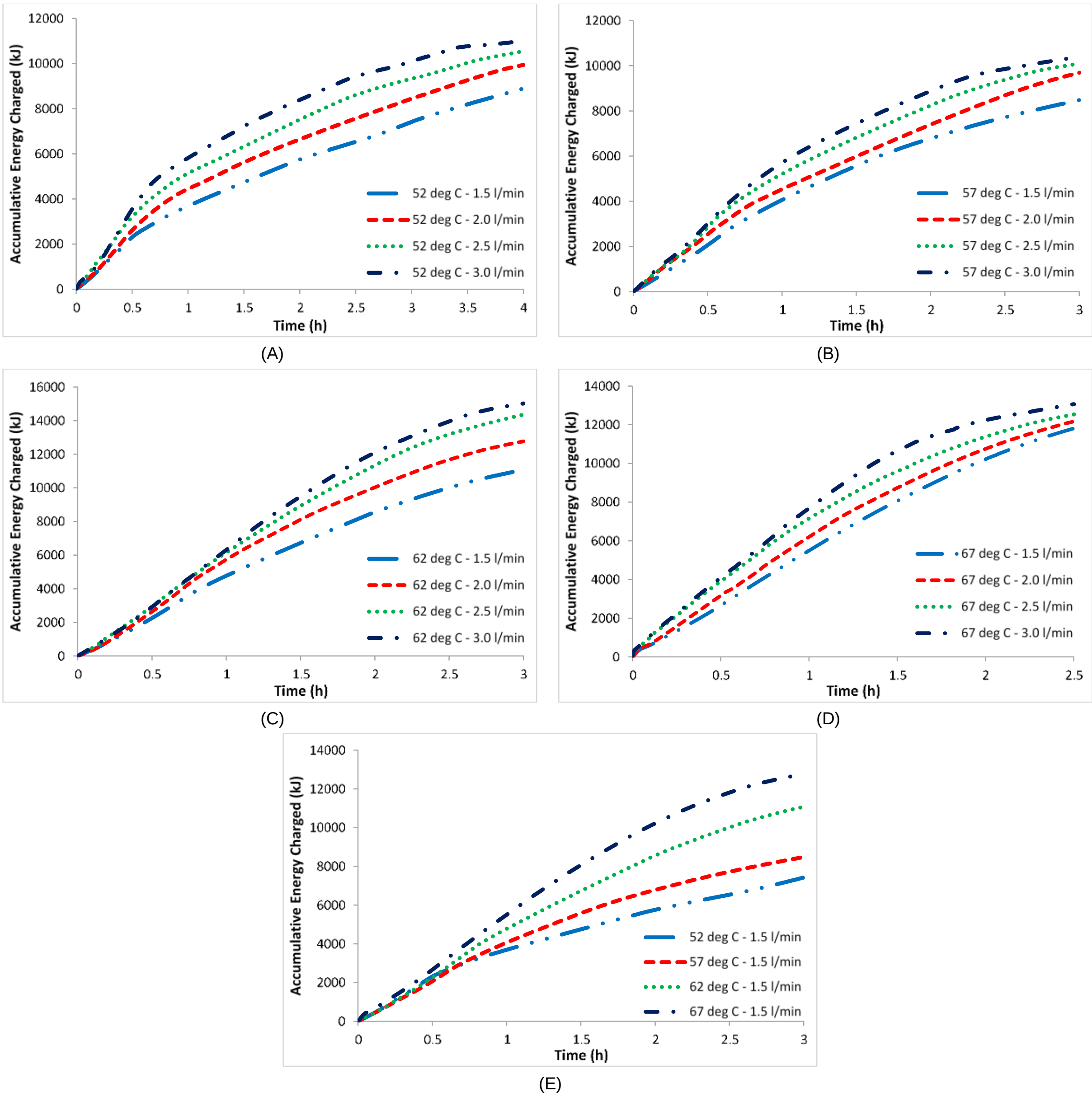

Fig. 5 Transient response of accumulative thermal energy storage during charging cycles at varied operating conditions of inlet temperatures and volume flow rates.

4.3. Discharging power and energy released

During open loop discharging cycles, the low temperature water is channelled through multi-tube passes to retrieve thermal energy from high temperature liquid paraffin in the shell container. Due to heat transfer to water, the enthalpy of liquid paraffin reduces and thus phase transition to solid state occurs. Transient local temperature response of paraffin to discharging cycles are registered by the thermocouples in the shell container and are discussed in detail in [23]. The set of twelve discharging cycles at varied operating conditions are listed in Table 4.

Instantaneous discharging power of paraffin is computed from enthalpy gradient of water at the inlet and outlet, as presented in Fig. 6. Similar to charging cycles, the time-wise discharging power can be categorised into three stages: a rapid increase in discharging power until maximum value is attained, a rapid but brief reduction in discharging power, followed by almost constant gradual declination towards the end of the discharging cycle. At initial stages of discharging cycle, the maximum discharging power is achieved due to higher temperature gradient between the water and paraffin. In the second stage, the sharp reduction in discharging power indicates formation of the solidified layer of paraffin over multi-tube passes and longitudinal fins. Low thermal conductivity of solid paraffin combined with restrained natural convection result in reduced discharging power. In the later stages, an almost constant gradual declination in discharging power is noticed as a result of reduced temperature gradient between the water and paraffin.

Moreover, the effect of varying operating conditions on discharging power is prominent. As presented in Fig. 6 (A), while discharging at constant inlet temperature of 5 ^{o}C, the maximum discharging power is augmented from 6.04 kW to 8.89 kW with an increase in volume flow rate from 1.5 l/min to 3 l/min, respectively. Likewise, in the case of discharging at constant inlet temperature of 10 ^{o}C and 15 ^{o}C, the maximum discharging power is improved from 5.75 – 9.56 kW and 5.18 – 10.37 kW with an increase in volume flow rate from 1.5 l/min to 3 l/min, respectively (see Fig. 6 (B) and (C)). Moreover, the influence of varying operating conditions on average discharging power is illustrated in Fig. 6 (D). It can be noticed that with an increase in temperature gradient by reducing inlet temperature from 15 ^{o}C to 10 and 5 ^{o}C and at constant volume flow rate of 3 l/min, the average discharging power is significantly enhanced by a fraction of 14.18% and 27.04%, respectively. Similarly, in case of constant inlet temperature of 10 ^{o}C, the average discharging power is augmented by 7.03%, 17.97% and 32.69% with an increase in volume flow rate from 1.5 l/min to 2, 2.5 and 3 l/min, respectively.

Further, the transient accumulative thermal energy retrieval from paraffin by water at varied operating conditions are illustrated in Fig. 7. It can be noticed that due to higher discharging power at the initial stages, the linear increment in thermal energy discharge is presented. Afterwards, the accumulative thermal energy retrieval is slowed down as discharging power declines which is indicated by curved increments. In the case of discharging at constant inlet temperature of 5 ^{o}C for 1.5 h, the accumulative energy retrieved by water is significantly increased from 10.74 MJ to 13.64 MJ with an increase in volume flow rate from 1.5 l/min to 3 l/min, as shown in Fig. 7 (A). With an increase in volume flow rate, the thermal resistance offered to convective heat transfer of water in the tube passes is reduced and consequently a higher amount of thermal energy is retrieved. Similarly, the rate of thermal energy discharge is significantly enhanced by increasing temperature gradient between inlet water and paraffin. As shown in Fig. 7 (D), the required time to discharge 12 MJ of thermal energy is significantly reduced from 2.12 h to 1.82 h and 1.54 h as the inlet temperature is decreased from 15 °C to 10 and 5 °C, respectively. Therefore, by adjusting the inlet operating conditions, the desired temperature and power needs can be attained at the outlet for utilisation in practical applications.

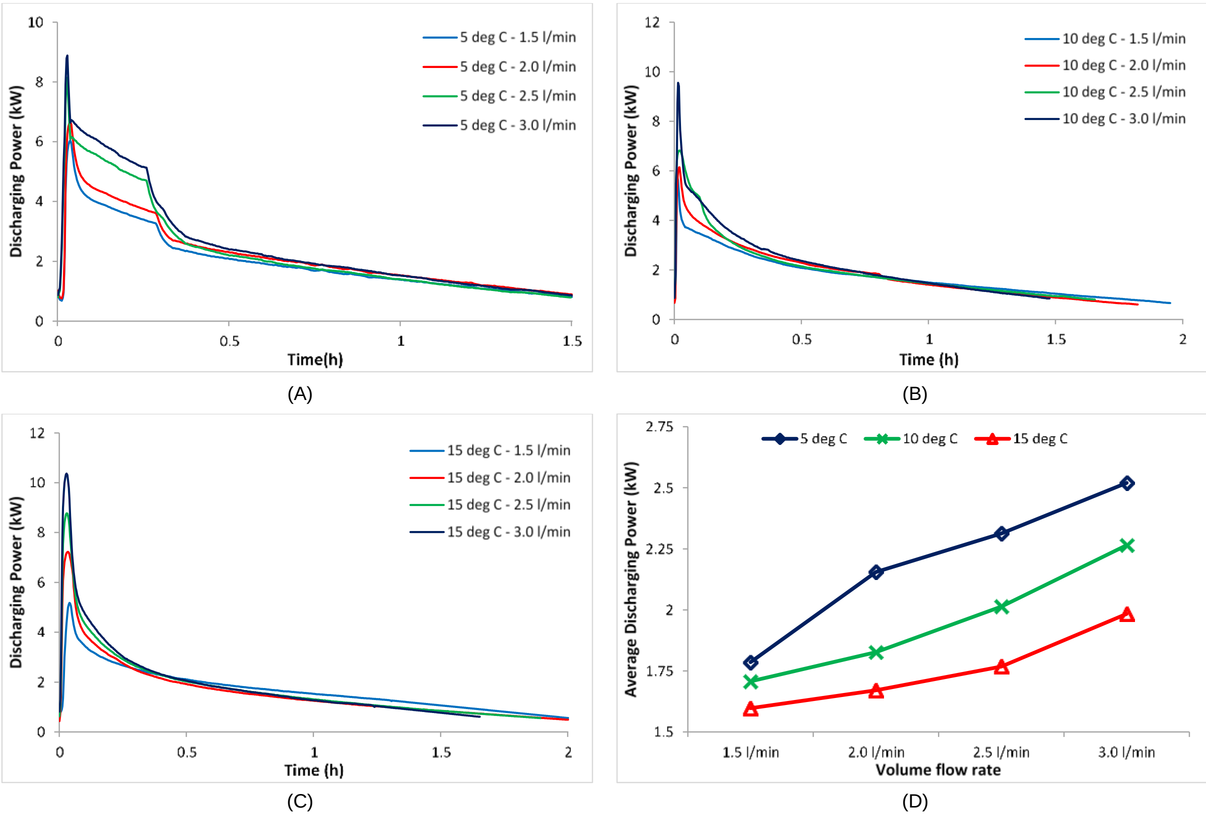

Fig. 6 Time-wise variation and average discharging power of the LHS unit while conducting discharging cycles at varied operating conditions.

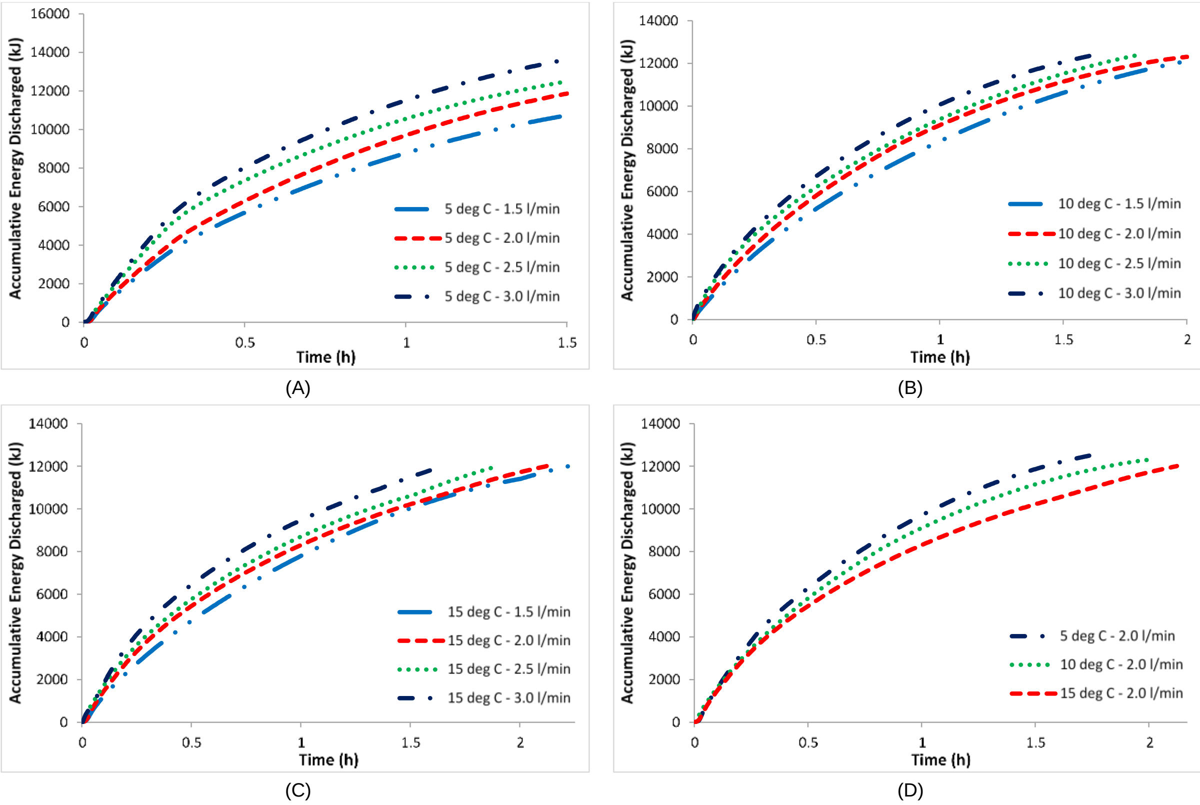

Fig. 7 Accumulative thermal energy retrieved from paraffin to water during discharging cycles at varied operating conditions.

4.4. Energy efficiencies of the LHS system

Thermal efficiencies of the LHS unit for various charging and discharging cycles are given in Table 5. During charging cycles, the range of charging efficiency increases with a rise in inlet temperature from 52 ºC to 62 ºC. However, the enhancement is minimal for further increase in inlet temperature from 62 ºC to 67 ºC. The range of charging efficiency is caused by imperfect thermal insulation of the LHS unit. Due to which some portion of thermal energy captured by paraffin is lost to the surrounding air. Therefore, the paraffin keeps on receiving thermal energy from incoming hot water until a steady state is reached. Steady state differs for various operating temperatures and thus the charging efficiency fluctuates [38]. In the case of discharging cycles, a relatively minimal variation in the range of discharging efficiency is noticed, with an average value of 84.92%. Furthermore, an increase in volume flow rate has presented an insignificant impact on charging/discharging efficiencies [29, 55].

Table 5
Thermal efficiencies of LHS unit during various charging/discharging cycles

	Operating conditions	η_c (%)		Operating conditions	η_d (%)
Charging cycles	$T_{in} = 52\ °C, \dot{V} = 2.5\ l/min$	79.29	Discharging cycles	$T_{in} = 05\ °C, \dot{V} = 2.0\ l/min$	83.92
	$T_{in} = 52\ °C, \dot{V} = 3.0\ l/min$	81.97		$T_{in} = 05\ °C, \dot{V} = 3.0\ l/min$	86.19
	$T_{in} = 62\ °C, \dot{V} = 1.5\ l/min$	79.13		$T_{in} = 10\ °C, \dot{V} = 1.5\ l/min$	85.68
	$T_{in} = 62\ °C, \dot{V} = 2.0\ l/min$	88.49		$T_{in} = 10\ °C, \dot{V} = 2.0\ l/min$	87.05
	$T_{in} = 62\ °C, \dot{V} = 2.5\ l/min$	97.31		$T_{in} = 10\ °C, \dot{V} = 2.5\ l/min$	87.58
	$T_{in} = 62\ °C, \dot{V} = 3.0\ l/min$	99.10		$T_{in} = 10\ °C, \dot{V} = 3.0\ l/min$	88.38
	$T_{in} = 67\ °C, \dot{V} = 2.5\ l/min$	98.69		$T_{in} = 15\ °C, \dot{V} = 2.0\ l/min$	80.82
	$T_{in} = 67\ °C, \dot{V} = 3.0\ l/min$	99.75		$T_{in} = 15\ °C, \dot{V} = 3.0\ l/min$	79.80

4.5. Effectiveness-NTU assessment of the LHS system

Average effectiveness provides better assessment of the specified design configuration of the LHS unit as compared to published data in the literature. It is measured during the phase transition duration of charging/discharging cycles, whereas sensible period of heat charge/discharge is neglected [48]. The sensitivity of average effectiveness to variable operating conditions of water is investigated during charging and discharging cycles, as shown in Fig. (8) and Fig. (9). It can be noticed that with an increase in volume flow rate, the average effectiveness for both charging and discharging cycles reduces. The maximum reduction in average effectiveness during charging and discharging cycles are recorded as 40.24% and 31.81%, respectively. With an increase in volume flow rate, the heat transfer coefficient is not proportionally increased [49]. Also, due to rapid circulation of water in multi-tube passes, less time is provided for proper heat transfer between the water and paraffin. As a result, the gradient between inlet and outlet temperature is reduced and thus, the average effectiveness is decreased. Furthermore, the impact of increasing inlet temperature on average effectiveness during charging/discharging cycles is prominent. The maximum enhancement in average effectiveness is noticed to be 65.72% and 32.62% for charging and discharging cycles, respectively.

Based on experimental calculation of average effectiveness at varied operating conditions, a non-linear regression technique is implemented to establish correlation between average effectiveness and mass flux at corresponding operating inlet temperature. The process flow diagram to develop correlations using non-linear regression technique is illustrated in Fig. 10. In the case of charging cycles, the correlation between average effectiveness and mass flux at respective inlet temperatures is given as follows:

$$\bar{\varepsilon}_{T_{in}=52°\mathrm{C}} = 1 - \exp\left(-0.01351 * \frac{A_{ext}}{\dot{m}}\right) \qquad R^2 = 0.9574 \qquad (26)$$

$$\bar{\varepsilon}_{T_{in}=57°\mathrm{C}} = 1 - \exp\left(-0.01679 * \frac{A_{ext}}{\dot{m}}\right) \qquad R^2 = 0.9517 \qquad (27)$$

$$\bar{\varepsilon}_{T_{in}=62°\mathrm{C}} = 1 - \exp\left(-0.02048 * \frac{A_{ext}}{\dot{m}}\right) \qquad R^2 = 0.9525 \qquad (28)$$

$$\bar{\varepsilon}_{T_{in}=67°\mathrm{C}} = 1 - \exp\left(-0.02439 * \frac{A_{ext}}{\dot{m}}\right) \qquad R^2 = 0.9239 \qquad (29)$$

Similarly, in case of discharging cycles, the correlations at respective three varied inlet temperatures are developed as follows:

$$\bar{\varepsilon}_{T_{in}=05°\mathrm{C}} = 1 - \exp\left(-0.01181 * \frac{A_{ext}}{\dot{m}}\right) \qquad R^2 = 0.9289 \qquad (30)$$

$$\bar{\varepsilon}_{T_{in}=10°\mathrm{C}} = 1 - \exp\left(-0.01305 * \frac{A_{ext}}{\dot{m}}\right) \qquad R^2 = 0.9403 \qquad (31)$$

$$\bar{\varepsilon}_{T_{in}=15°\mathrm{C}} = 1 - \exp\left(-0.01699 * \frac{A_{ext}}{\dot{m}}\right) \qquad R^2 = 0.9377 \qquad (32)$$

It can be noticed that the relevant charging/discharging correlations resemble the generalised correlation Eq. (17). Also, the constant C value is observed to be changing with respect to inlet temperatures for both charging and discharging cycles. Therefore, governing equations are developed for charging and discharging cycles to incorporate inlet temperature of water T_{in} and phase change temperature of paraffin T_m, as follows:

$$\bar{\varepsilon}_c = 1 - \exp\left\{-(0.00072(\mathrm{T}_{in} - \mathrm{T}_m) + 0.0061) * \frac{A_{ext}}{\dot{m}}\right\} \qquad R^2 = 0.9546 \tag{33}$$

$$\bar{\varepsilon}_d = 1 - \exp\left\{-(0.00052(\mathrm{T}_{in} - \mathrm{T}_m) + 0.0316) * \frac{A_{ext}}{\dot{m}}\right\} \qquad R^2 = 0.9281 \tag{34}$$

The governing equations for $\bar{\varepsilon}_c$ and $\bar{\varepsilon}_d$ enables prediction of the thermal performance of the design configuration of the LHS unit for PCMs other than paraffin RT44HC. For this reason, it is considered as an important development to determine the governing equation in evaluating average effectiveness for a particular PCM in the desired temperature range.

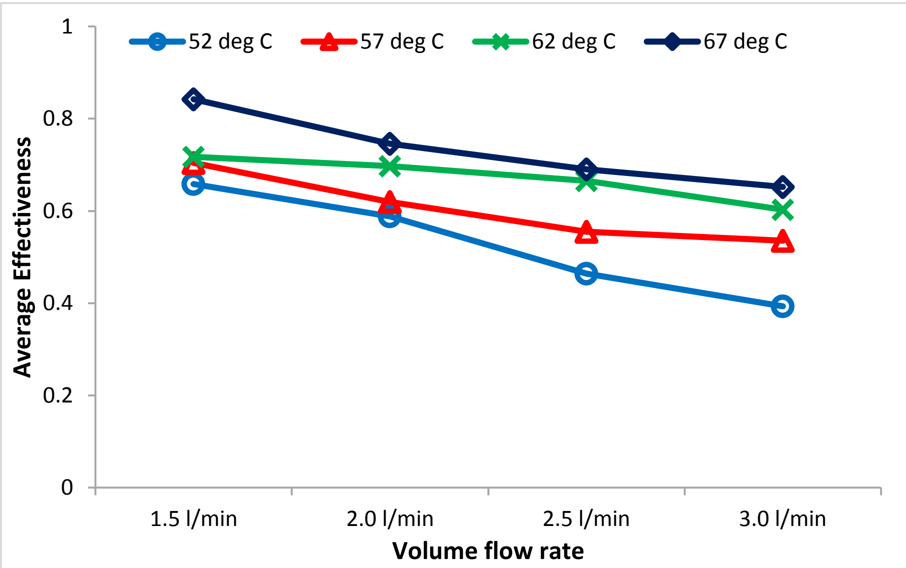

Fig. 8 Average effectiveness of the LHS unit at various charging cycles

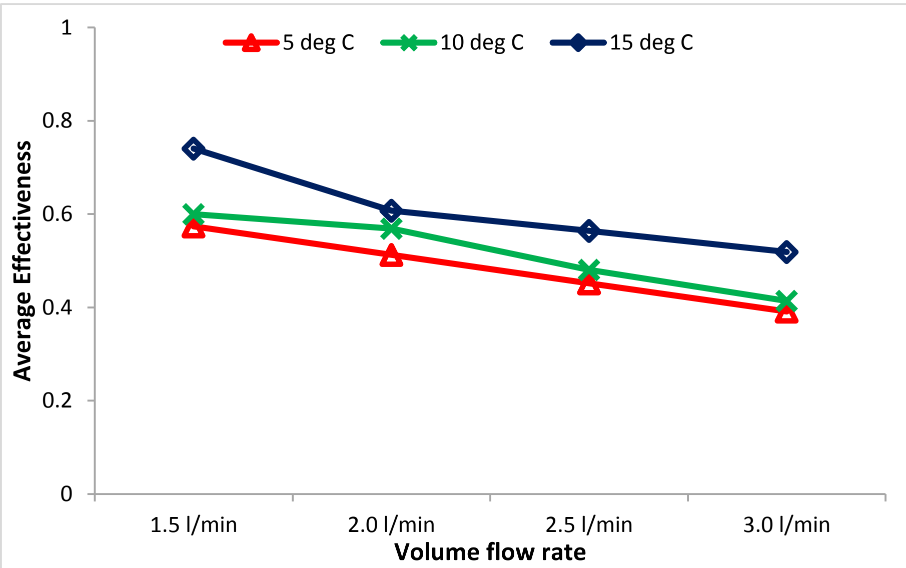

Fig. 9 Average effectiveness of the LHS unit at various discharging cycles

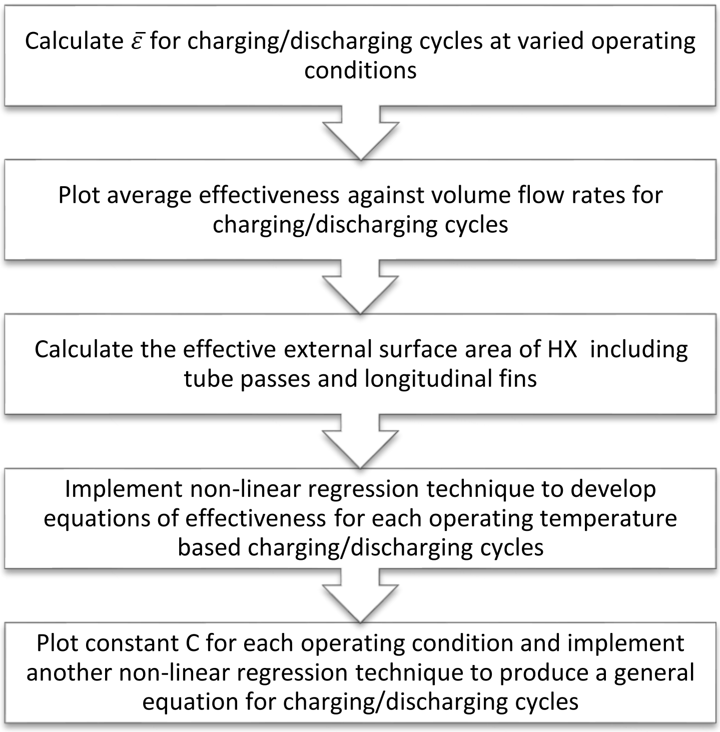

Fig. 10 Process diagram to produce governing equation for effectiveness of the LHS unit during charging and discharging cycles.

Further on, the thermal performance of the understudy design configuration is evaluated by comparing charging effectiveness with designs published in the literature, as shown in Fig. 11. The corresponding designs from literature includes: horizontal single shell-and-tube heat exchanger with paraffin by Hosseini et al. [56], four tubes-in-tank with salt hydrates by Tay et al. [48], U-shaped tubes-in-tank with copper foam and paraffin composite by Meng and Zhang [29], compact finned-tube heat exchanger with paraffin by Amagour et al.[38], horizontal multi-tubes with transversal squared fins in rectangular container with organic PCM by Gil et al. [57] and two copper pipes with four longitudinal fins in shell container with organic PCM by Murray and Groulx [45]. Fig. 11 illustrates that the current shell-and-tube heat exchanger with multi-tube passes and longitudinal fins design configuration has better thermal performance as compared to [38, 45, 48, 56, 57]. Therefore, it can be deduced that design optimisation and better orientation of extended surfaces are essential to achieve higher thermal performance. Moreover, the maximum charging effectiveness achieved by Meng and Zhang [29] is due to higher effective thermal conductivity of composite paraffin.

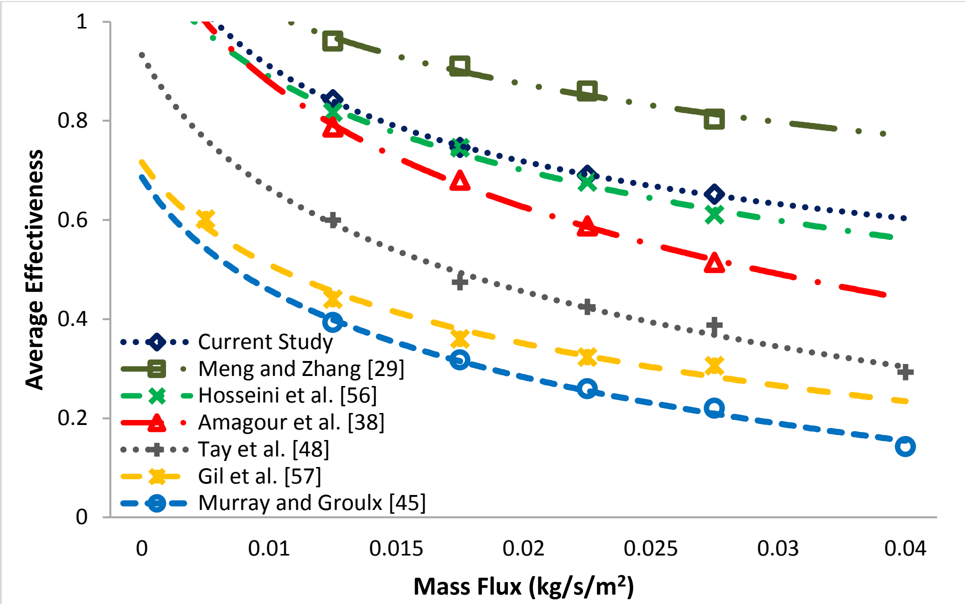

Fig. 11 Charging effectiveness of various LHS unit designs to examine comparative performance.

4.6. Natural convection characterisation

Thermal performance analyses of the longitudinal fins based LHS unit are conducted in terms of dominant mode of heat transfer. Impact of natural convection on phase transition process is evaluated by calculating Rayleigh number and Nusselt number from Eq. (18) – Eq. (23).

Transient response of Nusselt number to various charging cycles are illustrated in Fig. 12. At earlier stages, the Nusselt number peaks to maximum value due to higher charging power and is then followed by a sharp decline. These earlier stages are conduction dominant and the decline is due to formation of liquefied layers of paraffin around tube passes and longitudinal fins. Hence, the conduction heat transfer occurs through liquefied layers without any provision for natural convection. However, as the charging cycle progress, the amount of liquefied layers enlarge and buoyance driven natural convection intensifies. Due to escalation in natural convection, a moderate increase in Nusselt number is noticed until a local maxima is reached. As a result, the liquefied layers of paraffin ascend to upper region of shell container. In next stages, the accumulated liquefied layers of paraffin in upper region recirculate to reach the solid paraffin in lower region. However, due to congestion and stratification of liquefied paraffin in upper region, the influence of natural convection weakens. Hence, the Nusselt number gradually decline until the end of charging cycle.

Fig. 13 illustrates the experimental calculated values of Nu-Ra for charging cycles at varied operating conditions. Rayleigh numbers for charging cycles have ranged from 5.63×10^{10} – 1.37×10^{11}, which indicates that the melt front movement in upward direction is turbulent in nature. Moreover, the vertical orientation of longitudinal fins reinforces and supports natural convection in paraffin. For higher Rayleigh number, the buoyant forces surpass viscous forces and as a result, the Nusselt number and heat transfer coefficient are increased [58-60]. As a consequence, a higher charging rate with higher degree of thermal stratification of paraffin in the shell container can be obtained.

Rayleigh number is significantly enhanced with an increase in inlet temperature. For instance, while charging at constant volume flow rate of 1.5 l/min, the Rayleigh number is augmented by 32.25% with an increase in inlet temperature from 52 °C to 62 °C. Likewise, the Nusselt number is improved from 678.99 to 751.56, which indicates that natural convection is dominant mode of heat transfer at higher inlet temperatures. Conversely, it is observed that an increase in volume flow rate reduces the temperature gradient between the tube walls and the paraffin. Hence, the improvement in conduction heat transfer contributes to reduction in both Rayleigh and Nusselt numbers. For instance, with an increase in volume flow rate from 1.5 l/min to 3 l/min at constant inlet temperature of 62 °C, the Rayleigh and Nusselt numbers are reduced by 23.57% and 9.23%, respectively.

Based on experimental data, an empirical correlation between Nu-Ra is developed using non-linear regression technique, as follow:

$$\overline{Nu} = 0.122 * \overline{Ra}^{0.3404} \qquad 5.63 * 10^{10} \leq \overline{Ra} \leq 1.37 * 10^{11} \tag{35}$$

The coefficient of determination R^2 is 0.98, which illustrates excellent statistical fitting of regression line. In Eq. (35), the regression equation constant C and exponent n are in good congruence with the results established for vertical plates by Bergman et al. [44] ($\mathrm{C} = 0.1$ and $\mathrm{n} = 0.34$).

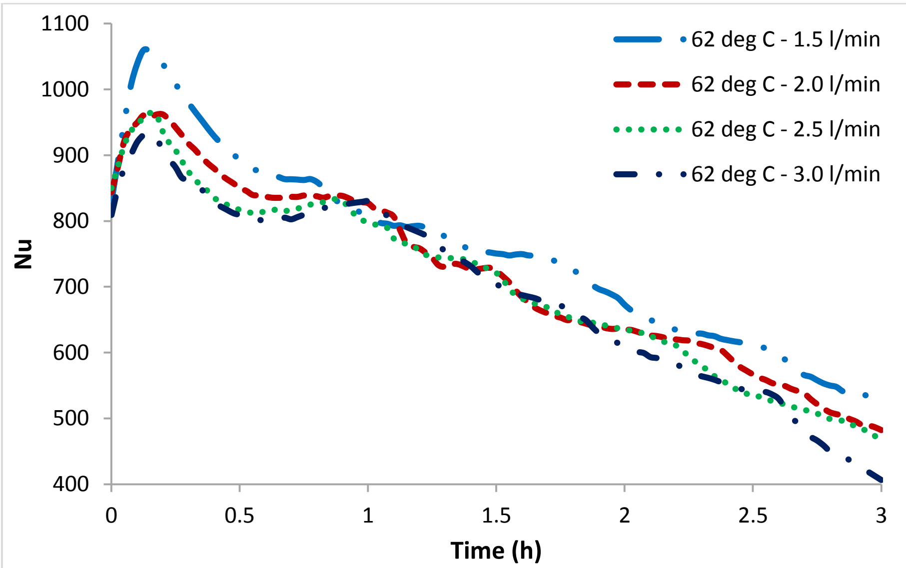

Fig. 12 Transient response of Nusselt number to charging cycles at constant inlet temperature and varying volume flow rates.

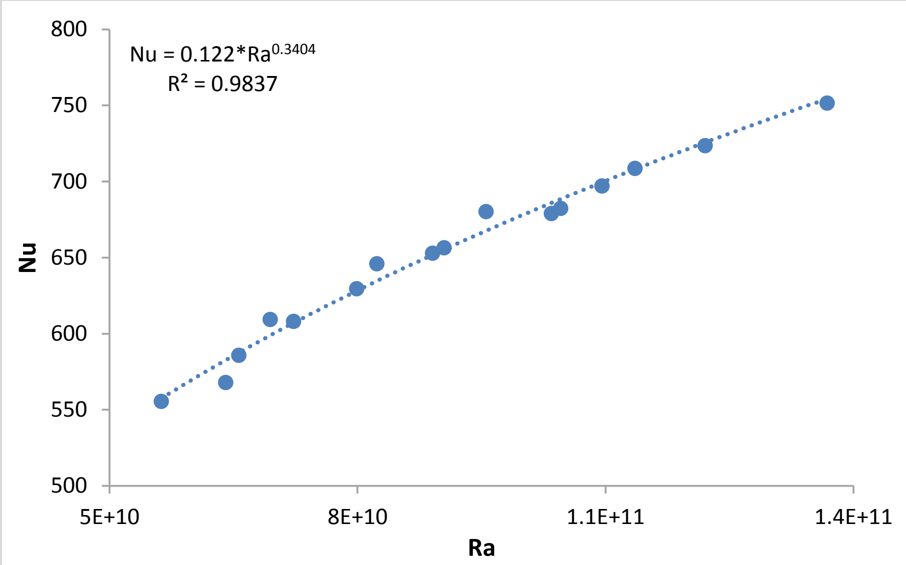

Fig. 13 Nu-Ra correlation is developed from experimental charging cycles at varied operating conditions.

4.7. Case studies of LHS system utilisation in practical applications

In order to implement the developed effectiveness correlations for design purposes in practical applications, two case studies are conducted. The effectiveness correlations can be implemented for a varied range of paraffin materials and operating conditions of water. However, in both case studies, the paraffin material and design features of the proposed LHS system are kept constant.

In the first case study, the viability of the proposed LHS systems in residential shower applications are assessed, as presented in Fig. 14 (A). As shown in Table 6, a number of design assumptions are made such as: T_{in} and T_{out} are fixed to 10 °C and 35 °C which are average municipal water temperatures in winter and hot water demand for the shower, respectively. The average flow rate of hot water during the shower is set to 5 l/min. Further on, the average discharge power and effectiveness are evaluated by computing Eq. (4) and Eq. (12), respectively. Subsequently, the design correlation Eq. (34) is implemented to determine the required effective heat transfer area to sustain continuous supply of hot water at the desired temperature. The calculated heat transfer area can be achieved by assembling four LHS systems in series to ensure hot water supply for service time of 60.97 min. The computed service time is sufficient for 6 people with an average shower time of 10 min.

In the second case study, the feasibility of the proposed LHS system integration with a radiator is examined, as shown in Fig. 14 (B). It is assumed that the outlet temperature from the LHS system is similar to the inlet temperature of radiators and vice versa. In order to sustain room temperature at 25 °C, the supply temperature to the radiator is set to 35 °C at a flow rate of 2 l/min, as presented in Table 6. Based on design assumptions, the average discharge power and effectiveness are calculated. It is deduced that a single LHS unit is capable of achieving control room temperature for two radiators installed in parallel in two separate rooms. Furthermore, the economic evaluations of the proposed LHS systems in practical applications are conducted. Table 7 shows the capital cost of unit LHS system, whereas, the payback periods of LHS systems as compared to electric and gas powered boilers are detailed in Table 8. To replace the electric boiler with the proposed LHS systems, the payback periods for both case studies are 5.5 years and 5 years. Similarly, to replace the gas powered boiler, the payback periods for both cases are 15.8 years and 8.1 years, respectively.

Table 6
Case studies of LHS unit implementation in domestic applications

Case Study	T_{in} (°C)	T_{out} (°C)	$\dot{V}$ (l/min)	$\dot{Q}$ (kW)	ε_{exp}	$A_{ext,r}$ (m²)	Required LHS units	$t_{service}$ (min)
6 x People Shower	10	35	5	8.69	0.735	7.94	4	60.97
2 x Parallel Radiators	25	35	2	1.39	0.526	0.94	1	68.51

Table 7
Capital cost of single LHS unit

Paraffin (RT44HC)	40 kg x 11.1 (£/kg)	£444.00
Copper Tank	100 L	£170.00
Copper Tube	8.2 m x 4.43 (£/m)	£36.33
Copper Fins	1.05 L x 151.74 (£/L)	£159.33
Welding		£15.99
Labour	8 h x 8.21 (£/h)	£65.68
Total capital cost (per unit)		£891.32

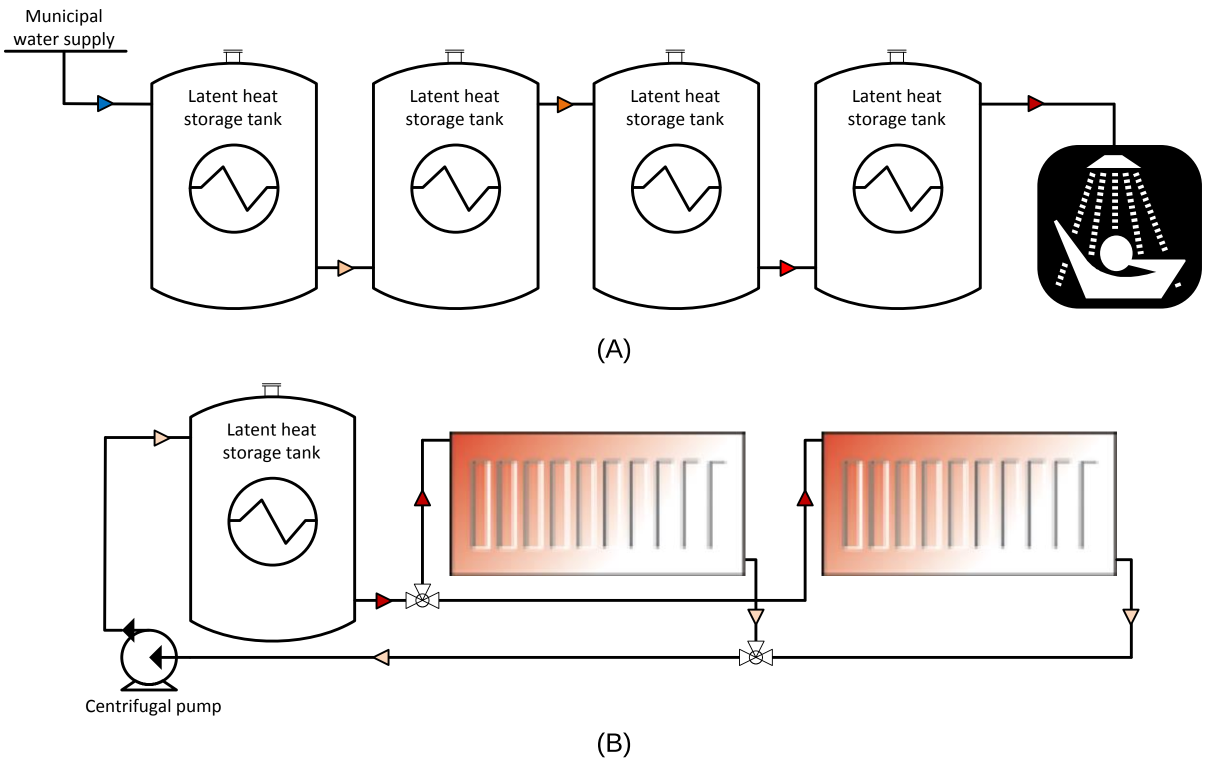

Fig. 14 Schematic representation of proposed LHS system utilisation in practical applications: (A) 1st case study and (B) 2nd case study.

Table 8
Payback period of proposed LHS system in domestic applications with two varied scenarios

		Case Study # 01 Shower	Case Study # 02 Radiator
Energy required (kJ)		31856.83	5727.44
Energy including boiler efficiency (90%) (kJ)		35042.51	6300.18
Total energy (kWh)		9.73	1.75
Scenario # 01			
Electric boiler cost (£/year)	15.75 (p/kWh)	£559.59	£100.61
Electricity standing charge (£/year)		£77.02	£77.02
Carbon dioxide factor (£/year)	0.305 (p/kWh)	£10.84	£1.95
Annual running cost (£/year)		£647.44	£179.57
Payback period (years)		5.5	5.0
Scenario # 02			
Gas boiler cost (£/year)	3.74 (p/kWh)	£132.88	£23.89
Gas standing charge (£/year)		£85.53	£85.53
Carbon dioxide factor (£/year)	0.184 (p/kWh)	£6.54	£1.18
Total annual running cost (£/year)		£224.95	£110.60
Payback period (years)		15.8	8.1

5. Conclusion

In this article, experimental analysis is conducted on commercial grade paraffin (RT44HC) in a shell-and-tube heat exchanger with multi-tube passes and longitudinal fins based LHS system. The LHS system is subjected to a series of sixteen close loop charging cycles with an integration to a flat plate solar collector and twelve open loop discharging cycles with a connection to the municipal water supply at varied operating conditions. Thermal performance of the designed LHS system is evaluated in terms of thermal energy storage/retrieval, average charging/discharging power, charging/discharging thermal efficiencies, heat transfer characterisation and average effectiveness. Moreover, the empirical correlations for charging/discharging effectiveness and Nu-Ra are derived to enable evaluation of the practical utilisation of the designed LHS system in domestic and commercial applications. The following specific conclusions are drawn from this experimental study:

- During charging/discharging cycles, the transient power is categorised into three stages as rapid increase until a maximum value is achieved, a brief rapid reduction is followed by a uniform and gradual reduction until the end of charging/discharging cycle. Likewise, the impact of increasing Stefan number on both charging/discharging power and accumulative thermal energy storage/retrieval is more pronounced as compared to increasing Reynolds number. For instance, the accumulative thermal energy storage is enhanced by 35.61% while charging at constant inlet temperature of 62 ^{o}C and increasing volume flow rate of 1.5 l/min to 3.0 l/min. Whereas, the accumulative thermal energy is augmented by 49.25% while charging at constant volume flow rate of 2 l/min and increasing inlet temperature from 52 ^{o}C to 62 ^{o}C. Furthermore, the inlet operating conditions can be regulated to achieve the desired charging/discharging power.

- An increase in volume flow rate has presented minimal influence on charging/discharging thermal efficiencies. However, the average effectiveness is significantly reduced with an increase in volume flow rate. For instance, the maximum reduction in charging and discharging average effectiveness are 40.24% and 31.81%, respectively. Moreover, the average effectiveness is significantly enhanced with an increase in temperature gradient for both charging and discharging cycles. Likewise, the average effectiveness of the current proposed LHS system is comparatively better than other several design configurations published in the literature. Also, the empirical correlations are developed to enable estimation of charging and discharging effectiveness for particular paraffin material and inlet temperature.
- The impact of design configurations of the shell-and-tube heat exchanger with vertical orientation of longitudinal fins on natural convection is evaluated by calculating Nu-Ra at varied operating conditions. Rayleigh number has ranged from 5.63×10^{10} – 1.37×10^{11}, which signifies the turbulent nature of melt front movement in upward direction. Moreover, it is noticed that with an increase in temperature gradient, the Rayleigh number is significantly enhanced and consequently, the Nusselt number and heat transfer coefficient are augmented. On the contrary, in the case of increasing volume flow rate, the Nu-Ra and heat transfer coefficient are noticeably reduced. Furthermore, the empirical correlation of Nu-Ra for the proposed shell-and-tube heat exchanger with longitudinal fins is in good agreement with established correlation for vertical plate.
- It is construed from case studies that the proposed LHS system can fulfil application based thermal energy demands by adjusting operating conditions or by assembling several units in series or parallel combinations. For instance, the effectiveness correlation is implemented to evaluate the feasibility of hot water supply for domestic usage and the integration of radiators for controlling the environment. The case study indicates that by assembling four LHS systems in series, the hot water supply demand for six people to shower can be fulfilled. Also, the integration of two parallel radiators with a single LHS system can sustain a controlled environment for more than an hour.

Acknowledgement

The authors would like to acknowledge Bournemouth University, UK and National University of Sciences and Technology (NUST), Pakistan for their financial assistance and in-kind support to conduct this research. Authors would also like to acknowledge in-kind support provided by Future Energy Source Ltd UK.

References

[1] REN21. Renewables 2017 Global Status Report, Paris: REN21 Secretariat, 2017.

[2] IEA. Energy and Climate Change International Energy Agency (IEA), 21st UN Conference of the Parties (COP21), Paris, 2015.

[3] M.Z. Jacobson. Review of solutions to global warming, air pollution, and energy security. Energy & Environmental Science. 2 (2009) 148-73.

[4] A. Sharma, V.V. Tyagi, C. Chen, D. Buddhi. Review on thermal energy storage with phase change materials and applications. Renewable and Sustainable energy reviews. 13 (2009) 318-45.

[5] A. Waqas, Z.U. Din. Phase change material (PCM) storage for free cooling of buildings—a review. Renewable and sustainable energy reviews. 18 (2013) 607-25.

[6] A. Modi, F. Bühler, J.G. Andreasen, F. Haglind. A review of solar energy based heat and power generation systems. Renewable and Sustainable Energy Reviews. 67 (2017) 1047-64.

[7] Z. Khan, Z. Khan, A. Ghafoor. A review of performance enhancement of PCM based latent heat storage system within the context of materials, thermal stability and compatibility. Energy Conversion and Management. 115 (2016) 132-58.

[8] N.S. Dhaidan, J. Khodadadi. Melting and convection of phase change materials in different shape containers: A review. Renewable and Sustainable Energy Reviews. 43 (2015) 449-77.

[9] J. Giro-Paloma, M. Martínez, L.F. Cabeza, A.I. Fernández. Types, methods, techniques, and applications for microencapsulated phase change materials (MPCM): a review. Renewable and Sustainable Energy Reviews. 53 (2016) 1059-75.

[10] L. Liu, D. Su, Y. Tang, G. Fang. Thermal conductivity enhancement of phase change materials for thermal energy storage: A review. Renewable and Sustainable Energy Reviews. 62 (2016) 305-17.

[11] J. Liu, C. Xu, X. Ju, B. Yang, Y. Ren, X. Du. Numerical investigation on the heat transfer enhancement of a latent heat thermal energy storage system with bundled tube structures. Applied Thermal Engineering. 112 (2017) 820-31.

[12] F. Agyenim, N. Hewitt, P. Eames, M. Smyth. A review of materials, heat transfer and phase change problem formulation for latent heat thermal energy storage systems (LHTESS). Renewable and sustainable energy reviews. 14 (2010) 615-28.

[13] M.K. Rathod, J. Banerjee. Thermal performance enhancement of shell and tube Latent Heat Storage Unit using longitudinal fins. Applied thermal engineering. 75 (2015) 1084-92.

[14] Z. Li, Z.-G. Wu. Analysis of HTFs, PCMs and fins effects on the thermal performance of shell–tube thermal energy storage units. Solar Energy. 122 (2015) 382-95.

[15] W.-B. Ye. Enhanced latent heat thermal energy storage in the double tubes using fins. Journal of Thermal Analysis and Calorimetry. 128 (2017) 533-40.

[16] W.-B. Ye. Melting process in a rectangular thermal storage cavity heated from vertical walls. Journal of Thermal Analysis and Calorimetry. 123 (2016) 873-80.

[17] A.A.R. Darzi, M. Jourabian, M. Farhadi. Melting and solidification of PCM enhanced by radial conductive fins and nanoparticles in cylindrical annulus. Energy Conversion and Management. 118 (2016) 253-63.

[18] S. Lohrasbi, M. Gorji-Bandpy, D.D. Ganji. Thermal penetration depth enhancement in latent heat thermal energy storage system in the presence of heat pipe based on both charging and discharging processes. Energy Conversion and Management. 148 (2017) 646-67.

[19] A. Caron-Soupart, J.-F. Fourmigué, P. Marty, R. Couturier. Performance analysis of thermal energy storage systems using phase change material. Applied Thermal Engineering. 98 (2016) 1286-96.
[20] M. Kabbara, D. Groulx, A. Joseph. Experimental investigations of a latent heat energy storage unit using finned tubes. Applied Thermal Engineering. 101 (2016) 601-11.
[21] Z. Khan, Z. Khan, K. Tabeshf. Parametric investigations to enhance thermal performance of paraffin through a novel geometrical configuration of shell and tube latent thermal storage system. Energy Conversion and Management. 127 (2016) 355-65.
[22] Z. Khan, Z.A. Khan. Experimental investigations of charging/melting cycles of paraffin in a novel shell and tube with longitudinal fins based heat storage design solution for domestic and industrial applications. Applied Energy. 206 (2017) 1158-68.
[23] Z. Khan, Z.A. Khan. An experimental investigation of discharge/solidification cycle of paraffin in novel shell and tube with longitudinal fins based latent heat storage system. Energy Conversion and Management. 154 (2017) 157-67.
[24] Y. Lin, Y. Jia, G. Alva, G. Fang. Review on thermal conductivity enhancement, thermal properties and applications of phase change materials in thermal energy storage. Renewable and Sustainable Energy Reviews. 82 (2018) 2730-42.
[25] X. Yang, J. Yu, Z. Guo, L. Jin, Y.-L. He. Role of porous metal foam on the heat transfer enhancement for a thermal energy storage tube. Applied Energy. 239 (2019) 142-56.
[26] X. Yang, Q. Bai, Z. Guo, Z. Niu, C. Yang, L. Jin, et al. Comparison of direct numerical simulation with volume-averaged method on composite phase change materials for thermal energy storage. Applied energy. 229 (2018) 700-14.
[27] X. Yang, Z. Guo, Y. Liu, L. Jin, Y.-L. He. Effect of inclination on the thermal response of composite phase change materials for thermal energy storage. Applied Energy. 238 (2019) 22-33.
[28] J.M. Mahdi, E.C. Nsofor. Multiple-segment metal foam application in the shell-and-tube PCM thermal energy storage system. Journal of Energy Storage. 20 (2018) 529-41.
[29] Z. Meng, P. Zhang. Experimental and numerical investigation of a tube-in-tank latent thermal energy storage unit using composite PCM. Applied Energy. 190 (2017) 524-39.
[30] Z. Khan, Z.A. Khan. Experimental and numerical investigations of nano-additives enhanced paraffin in a shell-and-tube heat exchanger: A comparative study. Applied Thermal Engineering. 143 (2018) 777-90.
[31] S. Lohrasbi, M. Sheikholeslami, D.D. Ganji. Discharging process expedition of NEPCM in fin-assisted latent heat thermal energy storage system. Journal of Molecular Liquids. 221 (2016) 833-41.
[32] M. Sheikholeslami, S. Lohrasbi, D.D. Ganji. Numerical analysis of discharging process acceleration in LHTESS by immersing innovative fin configuration using finite element method. Applied Thermal Engineering. 107 (2016) 154-66.
[33] M. Parsazadeh, X. Duan. Numerical study on the effects of fins and nanoparticles in a shell and tube phase change thermal energy storage unit. Applied Energy. 216 (2018) 142-56.
[34] K. Hosseinzadeh, M. Alizadeh, M. Tavakoli, D. Ganji. Investigation of phase change material solidification process in a LHTESS in the presence of fins with variable thickness and hybrid nanoparticles. Applied Thermal Engineering. 152 (2019) 706-17.
[35] M. Belusko, S. Sheoran, F. Bruno. Effectiveness of direct contact PCM thermal storage with a gas as the heat transfer fluid. Applied Energy. 137 (2015) 748-57.
[36] N. Tay, F. Bruno, M. Belusko. Comparison of pinned and finned tubes in a phase change thermal energy storage system using CFD. Applied Energy. 104 (2013) 79-86.

[37] A. López-Navarro, J. Biosca-Taronger, J. Corberán, C. Peñalosa, A. Lázaro, P. Dolado, et al. Performance characterization of a PCM storage tank. Applied Energy. 119 (2014) 151-62.
[38] M.E.H. Amagour, A. Rachek, M. Bennajah, M.E. Touhami. Experimental investigation and comparative performance analysis of a compact finned-tube heat exchanger uniformly filled with a phase change material for thermal energy storage. Energy Conversion and Management. 165 (2018) 137-51.
[39] N. Tay, M. Belusko, F. Bruno. An effectiveness-NTU technique for characterising tube-in-tank phase change thermal energy storage systems. Applied Energy. 91 (2012) 309-19.
[40] N.H.S. Tay, M. Belusko, A. Castell, L.F. Cabeza, F. Bruno. An effectiveness-NTU technique for characterising a finned tubes PCM system using a CFD model. Applied energy. 131 (2014) 377-85.
[41] H. Helvaci, Z.A. Khan. Mathematical modelling and simulation of multiphase flow in a flat plate solar energy collector. Energy Conversion and Management. 106 (2015) 139-50.
[42] Rubitherm® Technologies GmbH, http://www.rubitherm.eu/en/. 2018.
[43] MatWeb - Material Property Data, http://www.matweb.com/index.aspx. 2019.
[44] T.L. Bergman, F.P. Incropera, D.P. DeWitt, A.S. Lavine. Fundamentals of heat and mass transfer. John Wiley & Sons2011.
[45] R.E. Murray, D. Groulx. Experimental study of the phase change and energy characteristics inside a cylindrical latent heat energy storage system: Part 1 consecutive charging and discharging. Renewable energy. 62 (2014) 571-81.
[46] A. Sari, K. Kaygusuz. Thermal performance of palmitic acid as a phase change energy storage material. Energy Conversion and Management. 43 (2002) 863-76.
[47] H. El-Dessouky, F. Al-Juwayhel. Effectiveness of a thermal energy storage system using phase-change materials. Energy Conversion and Management. 38 (1997) 601-17.
[48] N. Tay, M. Belusko, F. Bruno. Experimental investigation of tubes in a phase change thermal energy storage system. Applied energy. 90 (2012) 288-97.
[49] Y. Allouche, S. Varga, C. Bouden, A.C. Oliveira. Experimental determination of the heat transfer and cold storage characteristics of a microencapsulated phase change material in a horizontal tank. Energy Conversion and Management. 94 (2015) 275-85.
[50] R. Kandasamy, X.-Q. Wang, A.S. Mujumdar. Transient cooling of electronics using phase change material (PCM)-based heat sinks. Applied Thermal Engineering. 28 (2008) 1047-57.
[51] S.W. Churchill, H.H. Chu. Correlating equations for laminar and turbulent free convection from a vertical plate. International journal of heat and mass transfer. 18 (1975) 1323-9.
[52] S.J. Kline. Describing uncertainty in single sample experiments. Mech Engineering. 75 (1953) 3-8.
[53] R.J. Moffat. Describing the uncertainties in experimental results. Experimental thermal and fluid science. 1 (1988) 3-17.
[54] H. Niyas, C.R.C. Rao, P. Muthukumar. Performance investigation of a lab-scale latent heat storage prototype–Experimental results. Solar Energy. 155 (2017) 971-84.
[55] P. Zhang, F. Ma, X. Xiao. Thermal energy storage and retrieval characteristics of a molten-salt latent heat thermal energy storage system. Applied energy. 173 (2016) 255-71.
[56] M. Hosseini, M. Rahimi, R. Bahrampoury. Experimental and computational evolution of a shell and tube heat exchanger as a PCM thermal storage system. International Communications in Heat and Mass Transfer. 50 (2014) 128-36.

[57] A. Gil, E. Oró, A. Castell, L.F. Cabeza. Experimental analysis of the effectiveness of a high temperature thermal storage tank for solar cooling applications. Applied Thermal Engineering. 54 (2013) 521-7.

[58] R. Elbahjaoui, H. El Qarnia. Transient behavior analysis of the melting of nanoparticle-enhanced phase change material inside a rectangular latent heat storage unit. Applied Thermal Engineering. 112 (2017) 720-38.

[59] M. Al-Jethelah, S.H. Tasnim, S. Mahmud, A. Dutta. Melting of nano-PCM in an enclosed space: Scale analysis and heatline tracking. International Journal of Heat and Mass Transfer. 119 (2018) 841-59.

[60] M. Prieto, B. González. Fluid flow and heat transfer in PCM panels arranged vertically and horizontally for application in heating systems. Renewable Energy. 97 (2016) 331-43.